Constraining the density dependence of the symmetry energy using the multiplicity and average p_T ratios of charged pions

M. D. Cozma*

Department of Theoretical Physics, IFIN-HH, Reactorului 30, 077125 Măgurele/Bucharest, Romania

(Received 14 March 2016; revised manuscript received 9 September 2016; published 3 January 2017)

The charged pion multiplicity ratio in intermediate-energy heavy-ion collisions, a probe of the density dependence of symmetry energy above the saturation point, has been proven in a previous study to be extremely sensitive to the strength of the isovector $\Delta(1232)$ potential in nuclear matter. As there is no knowledge, either from theory or experiment, about the magnitude of this quantity, the extraction of constraints on the slope of the symmetry energy at saturation by using exclusively the mentioned observable is hindered at present. It is shown that, by including the ratio of average p_T of charged pions $\langle p_T^{(\pi^+)}\rangle/\langle p_T^{(\pi^-)}\rangle$ in the list of fitted observables, the noted problem can be circumvented. A realistic description of this observable requires accounting for the interaction of pions with the dense nuclear matter environment by the incorporation of the so-called *S*-wave and *P*-wave pion optical potentials. This is performed within the framework of a quantum molecular dynamics transport model that enforces the conservation of the total energy of the system. It is shown that constraints on the slope of the symmetry energy at saturation density and the strength of the $\Delta(1232)$ potential can be simultaneously extracted. A symmetry energy with a value of the slope parameter $L > 50$ MeV is favored, at 1σ confidence level, from a comparison with published FOPI experimental data. A precise constraint will require experimental data more accurate than presently available, particularly for the charged pion multiplicity ratio, and better knowledge of the density and momentum dependence of the pion potential for the whole range of these two variables probed in intermediate-energy heavy-ion collisions.

DOI: 10.1103/PhysRevC.95.014601

I. INTRODUCTION

Pions produced in intermediate-energy heavy-ion collisions have been shown to provide promising means to study the isovector part of the equation of state (asy-EOS) of nuclear matter, commonly known as the symmetry energy (SE). The multiplicity ratio of charged pions (PMR) has been proven to be sensitive to the density dependence of SE [1], particularly to the density range of half to twice saturation density (ρ_0), with a maximum in sensitivity around $1.25\rho_0$ [2], while uncertainties in the isoscalar part of the equation of state are suppressed. This makes it suitable for extracting constraints for the value of the slope of the symmetry energy at saturation once its magnitude at saturation or at other particular density value is known from other sources (e.g., nuclear structure studies [3,4]). Higher order terms (e.g., curvature term and the associated $K_{\rm sym}$ parameter), while potentially important for the extrapolation of the symmetry energy to densities of interest for astrophysics studies, are customarily assumed to have a small effect and consequently simpler, one free parameter, parametrizations are adopted in heavy-ion transport calculations (e.g., the Gogny inspired MDI interaction [5]). The impact of SE on PMR has been shown to grow larger as the energy of the incident beam is decreased.

Attempts to constrain the slope of the SE at saturation by making use of various transport models and the experimentally measured value for the PMR in central ^{197}Au + ^{197}Au at an impact energy of 400 MeV/nucleon have resulted in a confusing picture: constraints on the high density dependence of the SE ranging from a very soft to a stiff one have been extracted [6–8], or even no sensitivity on the slope parameter has been reported [9]. Additionally, most models have led to a contradiction between the π^-/π^+ multiplicity ratio and neutron/proton elliptic flow ratio extracted constraints for the SE stiffness. Efforts to find a solution to this problem by studying the impact of in-medium modifications of the pion-nucleon interaction [10], the kinetic part of the SE term [11], the neutron skin thickness [12], or particle production threshold shifts due to the inclusion of self-energy contributions [13,14] on the PMR value have proven, from a quantitative point of view, largely unsuccessful, but some interesting findings were nevertheless reported.

The impact of including the self-energy contributions in the constraint of energy conservation that appears in the collision term of the transport equations, and thus implicitly modifying particle production thresholds, has been explored in Refs. [13,14]. Such an approach leads to a manifest implementation of energy conservation at local level; i.e., only the total energy of the particles involved in a binary reaction is conserved. It has lead to the interesting result that a stiffer asy-EOS leads to a slightly larger PMR than a soft choice would, which is opposite to the result obtained when the self-energy contributions to the energy conservation constraint are neglected. The effect was however found not to be quantitatively large enough to allow the extraction, from a comparison with experimental data, of the value for the slope L of the SE at saturation.

The next step was taken in Ref. [15], where a transport model which enforces the conservation of the total energy of the entire system during heavy-ion reactions has been developed. A restriction of the model to the so-called local

*dan.cozma@theory.nipne.ro

energy conservation scenario, which resembles the models of Refs. [13,14] closest (up to relativistic corrections of the dynamics) due to the relationship between self-energies and effective potentials (the latter being related to the real part of the former), has confirmed the results of those studies. The requirement of global total energy conservation was reported to have an important impact on pion multiplicities, particularly π^-, preserving the sensitivity of the PMR to the SE stiffness, but enhancing the effect of a higher multiplicity ratio for a stiffer asy-EOS reported in Ref. [14]. However, a large dependence of the PMR's magnitude on the strength of the isovector part of the $\Delta(1232)$ potential was evidenced, which, in view of the lack of information on this quantity, rendered this observable unsuitable for constraining the density dependence of the SE. This is in contrast with conclusions regarding the impact of the $\Delta(1232)$ potential on pionic observables reached in Refs. [16,17]. It is however not a conflict since in these lastly mentioned studies the threshold effects generated by the conservation of the total energy have not been accounted for, the impact of the $\Delta(1232)$ baryon arising only due to its motion in the mean field. Owing to the short lifetime of this resonance, the impact of its in-medium potential on pionic spectra is modest for values of the impact energy for which experimental data are available. Another important conclusion of the study in Ref. [15] was that for the standard choice for the strength of the isovector $\Delta(1232)$ potential, equal to that of the nucleon, an almost perfect agreement between the pion and elliptic flow extracted SE constraints could be obtained.

The present study extends the analysis performed in Ref. [15] to the average p_T ratio of charged pions, $\langle p_T^{(\pi^+)}\rangle/\langle p_T^{(\pi^-)}\rangle$ (PAPTR). It is shown that by using both observables, PMR and PAPTR, constraints on the stiffness of the SE can be extracted, independently of the strength of the isovector $\Delta(1232)$ potential. Constraints on the latter are naturally a by-product of such a study. To achieve this goal, the model of Ref. [15] is further improved by including the optical potential of pions in nuclear matter, both the so-called S- and P-wave components [18,19]. All the relevant details of this development are presented in Sec. II. The impact of this quantity on multiplicities, multiplicity spectra, and average p_T values of pions is studied in detail, and, where available, a comparison with experimental FOPI data [20–22] is presented. Additionally, the impact of poorer known model parameters is also investigated, followed by a presentation of the extracted constraints for SE (Sec. III). The article ends with a section devoted to summary and conclusions.

II. THE MODEL

A. The transport model

Heavy-ion collision dynamics is simulated using an upgraded version [15] of the Tübingen quantum molecular dynamics Model (QMD) transport model [23,24] which provides a semiclassical framework for the description of such reactions and accounts for relevant quantum aspects such as stochastic scattering and Pauli blocking of nucleons. It includes the production of all nucleonic resonances with masses below 2 GeV, in total 11 N^* and 10 Δ resonances. At energies of interest for this study pions are produced predominantly by the excitation of the $\Delta(1232)$ isobar in inelastic nucleon-nucleon collisions.

In QMD-type transport models, the total wave function of the ensemble of nucleons is taken to be the product of individual nucleon wave functions which are each represented by a Gaussian wave packet of finite spread in phase space. To make the transition to a semiclassical picture a formulation of quantum mechanics that is obtained by applying the Weyl transformation to the standard Schrödinger one is employed. The Wigner distribution, which is defined as the Weyl transform of the statistical density operator, is introduced. It represents the quantum analog of classical phase space densities with the exception that it can take both positive and negative values. With its help, it can be shown that the expectation values of the position and momentum operators satisfy the classical Hamiltonian equations of motion [25,26] which can be factorized to each particle given the ansatz made for the total wave function of the system,

$$\frac{d\vec{r}_i}{dt} = \frac{\partial\langle U_i\rangle}{\partial\vec{p}_i} + \frac{\vec{p}_i}{m}, \quad \frac{d\vec{p}_i}{dt} = -\frac{\partial\langle U_i\rangle}{\partial\vec{r}_i}. \tag{1}$$

Here, the average of the potential operator is understood to be taken over the entire phase space and weighted by the Wigner distribution of particle i. The potential operator U_i is in this case the sum of the Coulomb and strong interaction potential operators. In all kinematic equations the relativistic relation between mass, energy, and momentum is used.

The Gogny-inspired parametrization of the equation of state of nuclear matter [5] has been selected to describe the mean-field experienced by a nucleon at finite density. It leads to a mean-field nucleon potential,

$$\begin{aligned} U(\rho,\beta,p,\tau,x) = {} & A_u(x)\frac{\rho_{\tau'}}{\rho_0} + A_l(x)\frac{\rho_\tau}{\rho_0} + B\left(\frac{\rho}{\rho_0}\right)^\sigma(1-x\beta^2) \\ & - 8\tau x\frac{B}{\sigma+1}\frac{\rho^{\sigma-1}}{\rho_0^\sigma}\beta\rho_{\tau'} \\ & + \frac{2C_{\tau\tau}}{\rho_0}\int d^3\vec{p}\,'\frac{f_\tau(\vec{r},\vec{p}\,')}{1+(\vec{p}-\vec{p}\,')^2/\Lambda^2} \\ & + \frac{2C_{\tau\tau'}}{\rho_0}\int d^3\vec{p}\,'\frac{f_{\tau'}(\vec{r},\vec{p}\,')}{1+(\vec{p}-\vec{p}\,')^2/\Lambda^2}, \end{aligned} \tag{2}$$

that displays besides density (ρ) and isospin asymmetry (β) also a momentum (p) dependence in both the isoscalar and isovector components. The label τ designates the isospin component of the nucleon or resonance while the parameter x has been introduced to allow for an adjustment of the symmetry energy stiffness. The isovector part of the Gogny interaction is reproduced by setting $x = 1$. Negative and positive values of this parameter correspond to a stiff and a soft density dependence, respectively. The values of the $C_{\tau\tau}$, $C_{\tau\tau'}$, and Λ parameters are determined by optimally reproducing the momentum-dependent part of the Gogny interaction [5]. This results in an effective isoscalar nucleon mass of $0.7m_N$ and a neutron-proton effective mass splitting of approximately 0.4β at saturation density. The latter is in reasonable agreement

TABLE I. Values for L and $K_{\rm sym}$ coefficients appearing in the Taylor expansion of the symmetry energy around saturation density, $S(\rho) = S_0 + L/3u + K_{\rm sym}/18u^2 + \cdots$ with $u = \frac{\rho-\rho_0}{\rho_0}$ and $S_0 = 30.6$ MeV, for given values of the stiffness parameter x.

x	L (MeV)	$K_{\rm sym}$ (MeV)
−2	152	418
−1	106	127
0	61	−163
1	15	−454
2	−31	−745

with the average of values put forward by presently undisputed studies which have aimed at determining it from experimental data [27–30]. The remaining parameters are determined from the location of the saturation point (ρ_0), binding energy at saturation, magnitude of the symmetry energy at saturation ($S_0 = 30.6$ MeV), and value of the compressibility modulus ($K = 245$ MeV). To be complete, the determined values of all parameters appearing in the expression of the effective potential in Eq. (2) read

$$\begin{aligned} \Lambda &= 0.2630, \\ C_{\tau\tau} &= -0.0117, \quad C_{\tau\tau'} = -0.1034, \\ B &= 0.06844, \quad \sigma = 1.57065, \\ A_u(x) &= -0.05807 - \frac{2xB}{\sigma+1}, \\ A_l(x) &= -0.08266 + \frac{2xB}{\sigma+1}. \end{aligned} \tag{3}$$

The parameter σ is dimensionless, the rest being expressed in units of GeV. The first three parameters take the same values as in Ref. [5] while the others are different due to the chosen magnitude for the compressibility modulus. Values for the slope (L) and curvature ($K_{\rm sym}$) of the symmetry energy for selected values of x can be read from Table I.

In the previous version of the model, the radius mean square (rms) of initialized nuclei was determined solely from the position of the centroids of the wave function of nucleons. This is however inaccurate for the case of Gaussian-type nucleon wave functions of finite width, as used in QMD transport models, leading to an effective larger rms. The appropriate expression reads

$$\langle r^2 \rangle = \frac{1}{N} \sum_{i=1}^{N} (\langle \vec{r} \rangle - \vec{r}_i)^2 + \frac{3}{2} L_N, \tag{4}$$

where L_N is the square of the nucleon wave function width, the used convention for the parametrization of the nucleon wave function being the same as in Ref. [25]. The difference between the previously used and the appropriate value grows with increasing wave function width, reaching about 10% for values customarily used in transport models in connection with heavy nuclei. While the impact on pion multiplicities in central collisions is small, leaving the results of Ref. [15] unchanged, the impact on flow observables in mid-central and, especially, peripheral collisions is non-negligible. The somewhat larger values for the SE slope parameter at saturation extracted in Ref. [31] are corrected downwards by as much as 25 MeV, bringing the extracted constraints for the SE slope parameter from elliptic flow in Refs. [31,32] closer together. The value for the wave function width in this study is chosen to be $L_N = 4.33$ fm^2, guided by the ability of reproducing nuclear density profiles, particularly towards the surface of the nucleus.

In contrast to previous versions of the model, the pion is also associated a finite-width wave function, which is introduced for consistency reasons in order to evaluate the pion-nucleon Coulomb and density dependent strong interactions in the same fashion as their nucleon-nucleon counterpart. The value of the square of wave function width of the pion is set to half of that of the nucleon, $L_\pi = 0.5 L_N$, which is a close approximation of the experimentally measured squared ratio of their charge radii [33]. Additionally, the strength of the Coulomb interaction has been slightly adjusted (decreased by 10% compared to its standard value) in order to reproduce more closely, than in previous versions of the model, the Coulomb binding energy contribution to the empirical mass formula, which for ^{197}Au is approximately 3.72 MeV/nucleon [34]. This step is justified by the implicit dependence of the Coulomb interaction on the value of the wave function width of nucleons (and pions). The impact of this modification on pions is non-negligible, as will be shown in Sec. III, given its effective isovector nature, leading to lower values for both the PMR and the PAPTR. The value of the elliptic flow ratio of neutrons and protons is however only slightly modified.

Most of the results presented in this article have been obtained by enforcing conservation of the total energy of the system during a heavy-ion collision, by including potential energies in the energy conservation constraint imposed when determining the final state of a 2-body scattering, decay, or absorption process,

$$\sum_j \sqrt{p_j^2 + m_j^2} + U_j = \sum_i \sqrt{p_i^2 + m_i^2} + U_i, \tag{5}$$

both indexes running over all particles present in the system and corresponding, from left to right, to the final and initial states of an elementary reaction. This scenario has been referred to as the "global energy conservation" (GEC) scenario in [15]. Additionally, the "local energy conservation" (LEC) and "vacuum energy conservation" (VEC) scenarios have been introduced. They correspond to the situation when only the potential energies of the particles directly involved in the 2-body scattering, decay, or absorption process are accounted for in the energy conservation constraint and when the potential energies of particles in the medium are ignored in the collision term, respectively. For further details about these approximations the reader is referred to Ref. [15].

It will prove useful to mention the used ansatz for the potential of $\Delta(1232)$ and heavier baryonic resonances, derived under the assumption that it is given by the weighted average of that of neutrons and protons, the weight for each charge state being equal to the square of the Clebsch-Gordon coefficient for isospin coupling in the process $\Delta \to \pi N$ [35]. It can be

cast in the following form,

$$\begin{aligned} V_{\Delta^-} &= V_N + (3/2)V_v, \\ V_{\Delta^0} &= V_N + (1/2)V_v, \\ V_{\Delta^+} &= V_N - (1/2)V_v, \\ V_{\Delta^{++}} &= V_N - (3/2)V_v, \end{aligned} \tag{6}$$

where V_N and V_v are the isoscalar nucleon potential and the difference between the potentials of two neighboring isospin partners, respectively. With the assumptions presented above, it can be shown that $V_v = \delta$, with the definition $\delta = (1/3)(V_n - V_p)$. By varying the magnitude of V_v different scenarios for the strength of the isovector baryon potential can be explored. The choices $V_v = -2\delta$, $-\delta$, 0, δ, 2δ, and 3δ will be used in this study. The last choice leads, in the case of a momentum independent potential, to no threshold effects. The results of this case for the PMR resemble that of transport models that do not take into account the potential energies in the energy conservation constraint in collision, decay, or absorption processes [15].

B. The pion optical potential

Theoretical and experimental studies of the pion-nucleus interactions date back to the 1950s. Theoretically motivated parametrizations of the so-called pion optical potentials introduced back then [18,19] are still in current use when comparing different versions of the potential derived either theoretically from microscopical models [41–44] or extracted from a comparison of effective models to experimentally measured data for pion-nucleus scattering [37,45,46] or properties of pionic atoms [36,47,48]. The last mentioned studies have also been motivated by the opportunity to investigate a possible partial restoration of chiral symmetry in nuclei via a modification of the isovector S-wave πN scattering amplitude [48–52].

A commonly used parametrization for the pion optical potential in the context of studying pionic atoms, introduced by Ericson and Ericson [19], reads

$$V_{\rm opt}(r) = \frac{2\pi}{\mu}\left[-q(r) + \vec{\nabla}\frac{\alpha(r)}{1+\frac{4}{3}\pi\lambda\alpha(r)}\vec{\nabla}\right], \tag{7}$$

where

$$\begin{aligned} q(r) &= \epsilon_1(\bar{b}_0\rho + \bar{b}_1\beta\rho) + \epsilon_2 B_0\rho^2, \\ \alpha(r) &= \epsilon_1^{-1}(c_0\rho + c_1\beta\rho) + \epsilon_2^{-1}(C_0\rho^2 + C_1\beta\rho^2). \end{aligned}$$

In the above expressions μ is the reduced mass of the pion-nucleus system and λ is the Lorentz-Lorentz correction parameter which accounts for the impact of short-range nucleon-nucleon correlations on the potential. The extra parameters are defined as follows: $\epsilon_1 = 1 + m_\pi/m_N$, $\epsilon_2 = 1 + m_\pi/2m_N$, with m_π and m_N the π-meson and nucleon masses, respectively. Coordinate dependence of the potentials enters through the expressions for the density ρ and the isospin asymmetry β. The parameters $\bar{b}_0$, $\bar{b}_1$, and B_0 determine the strength of the S-wave part of the interaction, while the P-wave term is described by the ones labeled c_0, c_1, C_0, and C_1. Parameters denoted by capital letters can have both a real and an imaginary part while the others are real. During the last decades, many sets for the optical potential parameter values have been extracted by fitting available experimental data, mainly pionic atom properties and pion-nucleus scattering cross sections. Some differences do however exist between the many available sets for each parameter and are understood as being due to differences in the fitting procedure, some small correction terms (e.g., angular transformation terms, Pauli blocking, and Fermi averaging [45]) included or omitted by the various analyses or somewhat different experimental data sets. A limited number of such parameter sets, which were used in the present study, are presented in Table II. A more comprehensive list can be found in Ref. [36] from where the entries listed in Table II were selected.

As pointed out by several authors [37,45,53,54], the density regimes probed in pionic atoms and elastic pion-nucleus scattering experiments are $0.5\rho_0$–$0.75\rho_0$ and $0.0\rho_0$–$0.5\rho_0$, respectively. For the pionic atoms case also the momentum of the pion is drastically limited to $p < 0.050\,\text{GeV}/c$ (or equivalently pion kinetic energies $\omega < 9\,\text{MeV}$). Extrapolating the pion potentials to values of these two variables probed in heavy-ion collisions of impact energies in the range 200–500 MeV/nucleon ($0.0\rho_0$–$2.5\rho_0$ for density and 0.0–0.3 GeV/c for pion momentum) leads to unavoidable inaccuracies which originate from the noted differences in the potential parameter values and may be viewed as model dependence. An attempt will be made to estimate its magnitude by determining the observables of interest for different choices of the pionic potentials.

Alternatively, the pion optical potential can be determined theoretically within the framework of effective hadronic models. Starting from basic interaction terms for the πNN, $\pi N\Delta$, and in some cases also $\pi NN^*(1440)$ vertices one can determine the pion potential by computing the in-medium

TABLE II. A small sample of the pion optical potential parameter sets extracted from experimental pionic atom data available in the literature. The entries in this table are a subset of the ones presented in Table II of Ref. [36], the labeling being identical. The selection was made such as to cover as much as possible, with a limited number of parameter sets, of the range of the S- and P-wave isoscalar and isovector potential strengths extracted from data. The original references for these parameter sets are Ref. [37] for SM-1 and SM-2, Ref. [38] for Batty-1, Ref. [39] for Batty-2, and Ref. [40] for Konijn-2.

	$\bar{b}_0$ (m_π^{-1})	$\bar{b}_1$ (m_π^{-1})	ReB_0 (m_π^{-4})	ImB_0 (m_π^{-4})	λ	c_0 (m_π^{-3})	c_1 (m_π^{-3})	ReC_0 (m_π^{-6})	ImC_0 (m_π^{-6})
SM-1	−0.0283	−0.120	0.0	0.042	1	0.223	0.250	0.0	0.10
SM-2	0.030	−0.143	−0.150	0.046	1	0.210	0.180	0.11	0.09
Batty-1	−0.017	−0.130	−0.048	0.0475	1	0.255	0.170	0.0	0.09
Batty-2	−0.023	−0.085	−0.021	0.049	1	0.210	0.089	0.118	0.058
Konijn-2	0.025	−0.094	−0.265	0.0546	1	0.273	0.184	−0.140	0.105

TABLE III. Free-space values of the isoscalar and isovector strengths of the πN center-of-mass scattering amplitudes, b_0 and b_1.

	$b_0\ (m_\pi^{-1})$	$b_1\ (m_\pi^{-1})$
Exp	$-0.0001^{+0.0009}_{-0.0021}$	$-0.0885^{+0.0010}_{-0.0021}$
ChPT	0.0076 ± 0.0031	-0.0861 ± 0.0009
WT	0.0	-0.0790

pion self-energy in a perturbative approach, the lowest order corresponding to a linear density approximation when the energy dependence of the interaction is neglected. Models that go beyond the lowest order in density are available in the literature, both for S-wave [42–44,53,55] and P-wave [42,43,56] components of the potential. Their validity is restricted to subsaturation densities and for the most sophisticated ones [43,44] also to rather low values of the pion kinetic energy, $\omega < 50$ MeV. Problems similar to the ones noted above occur also when attempting to use these theoretically determined potentials in simulations of intermediate-energy heavy-ion collisions.

Extrapolations of the empirically or theoretically derived potentials to pion kinetic energies and densities higher than the ones they are appropriate for must proceed with care. The treatment of the S- and P-wave components is necessarily different. The case of the S-wave potential will be considered at first. As already mentioned, the original goal of studying pionic atoms was to investigate the possibility of a partial restoration of chiral symmetry inside dense nuclear matter. To this end, the isoscalar and isovector πN center-of-mass scattering amplitudes at threshold in dense nuclear matter, $\bar{b}_0$ and $\bar{b}_1$, need to be compared to their free-space counterparts, b_0 and b_1. For these latter ones the extracted values from pionic hydrogen and deuterium x-ray experiments [57] and theoretical predictions from chiral perturbation theory (ChPT) [58,59] agree reasonably well and are moreover well approximated by the Weinberg-Tomozawa (WT) lowest-order chiral limit, as presented in Table III.

Initial extraction of the values of $\bar{b}_0$ and $\bar{b}_1$ (at finite density) from experimental data of pionic atoms revealed an unusually large repulsion in the isoscalar channel [60], as is also evident from Table II, which seemed to contradict the expectation of how chiral symmetry restoration is realized in nature. It was later recognized that, for the isoscalar channel, double-scattering contributions play a crucial role due to cancellations in the single scattering amplitude that lead to an almost zero isoscalar term at leading order in the chiral expansion. Consequently, most of the magnitude of $\bar{b}_0$ at finite density originates from the isovector term due to identical particle correlations in nuclear matter leading to the relation

$$\bar{b}_0 = b_0 - \frac{3}{2\pi}\left(b_0^2 + 2b_1^2\right)\left(\frac{3\pi^2}{2}\rho\right)^{1/3}, \tag{8}$$

which needs to be supplement by additional less well understood corrections, such as coherent neutron and proton scattering lengths or dispersive effects of nuclear pion absorption, in order for a quantitative agreement to be reached [61].

The expressions for the leading order approximation in a pion mass expansion of b_0 and b_1 in ChPT using the Weinberg-Tomozawa interaction term [62,63],

$$b_0 = 0.0, \quad b_1 = -\frac{m_\pi}{8\pi(1.0 + m_\pi/m_N)f_\pi^2}, \tag{9}$$

suggest that in-medium effects on the πN scattering amplitude enter via a modification, with density, of the value of the pion decay constant f_π, for which the following relation holds for small densities [64,65]:

$$f_\pi^2(\rho) = f_\pi^2(0) - \frac{\sigma\rho}{m_\pi^2}, \tag{10}$$

where $\sigma = 45 \pm 8$ MeV is the well-known pion-nucleon σ term, leading to an effective dependence of b_1 on density,

$$b_1(\rho) = \frac{b_1}{1 - \frac{\sigma\rho}{m_\pi^2 f_\pi^2}} \simeq \frac{b_1}{1 - 2.3\rho}. \tag{11}$$

Using these considerations it can be shown that a satisfactory description of pionic atoms and pion-nucleus elastic scattering can be achieved with values for b_0 and b_1 in Eq. (8) compatible with the vacuum ones listed in Table III, once the energy dependence of the πN amplitudes and realistic neutron and protons density profiles inside the nucleus are also taken into account [52,66,67]. It can be additionally shown that, by enforcing gauge invariance by minimal substitution in the Klein-Gordon equation used to describe pionic atoms, S-wave pion potentials with $\mathrm{Re}B_0 = 0.0$ (in units of m_π^{-4}) are compatible with experimental data with the magnitude of the imaginary partly largely unaffected by any of the details of the scenario employed [68].

As mentioned in the previous paragraph, the energy dependence of the S-wave potential is also important for the description of experimental data away from threshold (pion-nucleus scattering). In the leading order approximation of ChPT (pion kinetic energy smaller than pion rest mass) the dominant energy dependence originates from b_0. This result is supported by the energy dependence of empirical free-space πN amplitudes that have been extracted from experimental data (see for example Ref. [69]), which advocate slopes of the potential parameters b_0 and b_1 of $-0.00053\ m_\pi^{-1}$/MeV and a negligible one, respectively. Analyses of low-energy pion-nucleus scattering arrive at a qualitatively identical conclusion [37,45,46], additionally presenting evidence of a dampening of the energy dependence of the isoscalar term of the S-wave scattering amplitudes in nuclear matter as compared to free space.

Consequently, in the simulations presented in the next section the values of b_0 and its slope were chosen with the conservative requirement of satisfying the experimental constraints derived from pion-nucleus scattering for the so-called effective isoscalar scattering amplitude $\bar{b}_0^{\mathrm{eff}}$ [53]: $b_0 = -0.010\ m_\pi^{-1}$ and $db_0/dE_{\mathrm{kin}} = -0.00016\ m_\pi^{-1}$/MeV. It is defined as $\bar{b}_0^{\mathrm{eff}} = \bar{b}_0 + \rho^{\mathrm{eff}}\mathrm{Re}B_0$ [37], neglecting small corrections proportional to the ratio between the pion kinetic energy and the mass of the nucleus under consideration, with ρ^{eff} being the effective density at which the potential needs to be evaluated at a given pion kinetic energy.

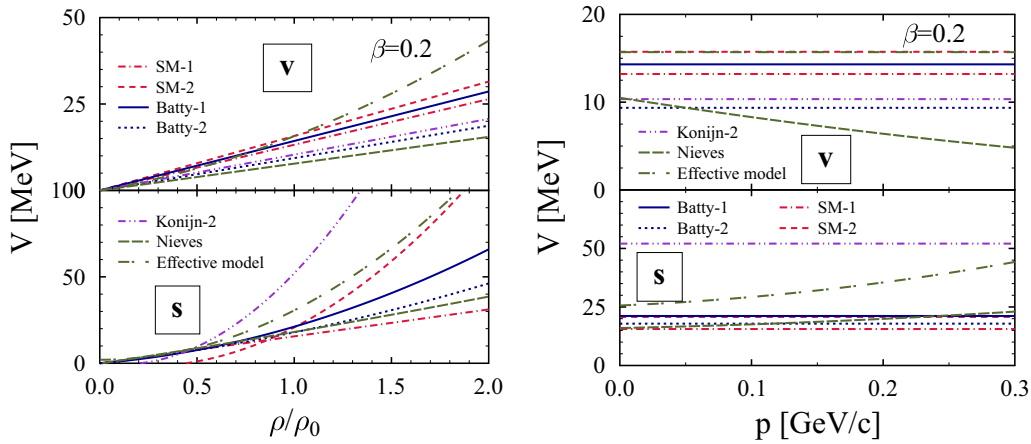

FIG. 1. Density dependence of the pionic S-wave potential at fixed momentum, $p = 0.125$ GeV/c (left-hand panels), and its momentum dependence at fixed density, $\rho/\rho_0 = 1.0$ (right-hand panels). The total S-wave potential has been split into its isoscalar (bottom panels, labeled "s") and isovector (top panels, labeled "v") components. In addition to the potentials extracted from pionic atom data, the behavior of the theoretical model of Nieves *et al.* [43] and of the chiral perturbation theory inspired effective model discussed in the text are also presented. The value of the isospin asymmetry parameter has been set to $\beta = 0.20$, close to that of the ^{197}Au nuclei for which the heavy-ion simulations have been performed.

This approach accounts, even though in a rather qualitative manner, for modifications, induced by the dense medium, of the slopes of the energy dependence of the parameters of the potential. The nonzero value of b_0, different from its free-space value (see Table III), effectively accounts for the omitted corrections in the process of deriving Eq. (8) [61] at finite density. The described procedure to account for the energy dependence of the pion-nucleon scattering amplitudes resembles the approach employed in pionic atom studies [68]. The analytical dependence on energy of the theoretical S-wave pion potential of Ref. [43] is however different, leading to a smaller energy slope of $\bar{b}_0$ but to an energy-dependent $\bar{b}_1$ (see the right panel of Fig. 1).

The following S-wave potential will be used in the numerical simulations of heavy-ion collisions, if not otherwise stated. For b_0 the value of the slope extracted above from experimental pion-nucleus elastic scattering will be used, while for b_1 a linearized approximation of Eq. (11), that is applicable (nonsingular) to the entire density interval probed by intermediate-energy heavy-ion collisions, will be employed:

$$b_0(\omega) = -0.010 - 0.00016\omega,$$
$$b_1(\rho) = -0.088\left(1 + \frac{0.6116}{b_1}\frac{\rho}{\rho_0}\right). \qquad (12)$$

Both potential parameters in the expressions above are expressed in units of m_π^{-1}, while the kinetic energy of the pion, ω, is expressed in units of MeV. The values of the parameters entering in Eq. (7) are determined from Eq. (8) for $\bar{b}_0$ and $\bar{b}_1 = b_1(\rho)$ for $\bar{b}_1$. It needs to be stressed that the above choice for b_1 [together with the one in Eq. (11)] may not be a very good approximation far away from the low-density region; however neglecting the density dependence of b_1 completely may arguably be a worse approximation. The precise (realistic) dependence on density of $\bar{b}_1$ for the entire density domain of interest in this study is presently unknown and any extrapolation of low-density ChPT results of the type of the one in Eq. (12) introduces unavoidable uncertainties in the results.

The discussion of the S-wave potential is concluded by presenting, in Fig. 1, the density (left panel) and momentum (right panel) dependence of the empirical S-wave potentials of Table II, of the theoretical model of Nieves *et al.* [43] and the effective model presented above. The isoscalar and to a lesser extent also the isovector components are compatible with each other in the density region probed in pionic atom experiments; their strengths differ however substantially in the suprasaturation region. Only the theoretical and effective models for the S-wave pion potential present a momentum dependence, which are rather different from each other, the latter having a stronger dependence in the isoscalar channel and none for the isovector case.

Turning to the P-wave potential, one can notice from Table II that, by using the concept of effective density [37], the various sets of potentials extracted from pionic atoms present isoscalar components of similar strength, while for the isovector term c_1 the strength varies, in absolute magnitude, by a factor of three and consequently also the ratio of the strengths of the isovector and isoscalar components varies within a similar range. This is visible in the left panel of Fig. 2 where the density dependence of the isoscalar and isovector P-wave potentials at a value of the pion momentum $p = 0.125$ GeV is presented. Additionally, two theoretical pion P-wave pion potentials are also depicted, whose strength is systematically smaller than that of the empirical ones extracted from pionic atoms data. It is expected that the mentioned differences may have an important impact on observables that probe the isovector part of the interaction. The strong dependence of the P-wave potential on pion momentum and the rather important dependence of the average pion momentum on the isospin in heavy-ion collisions lead to an effective isovector behavior also of the isoscalar P-wave terms. This fact stresses the importance of an accurate knowledge of the pion potential.

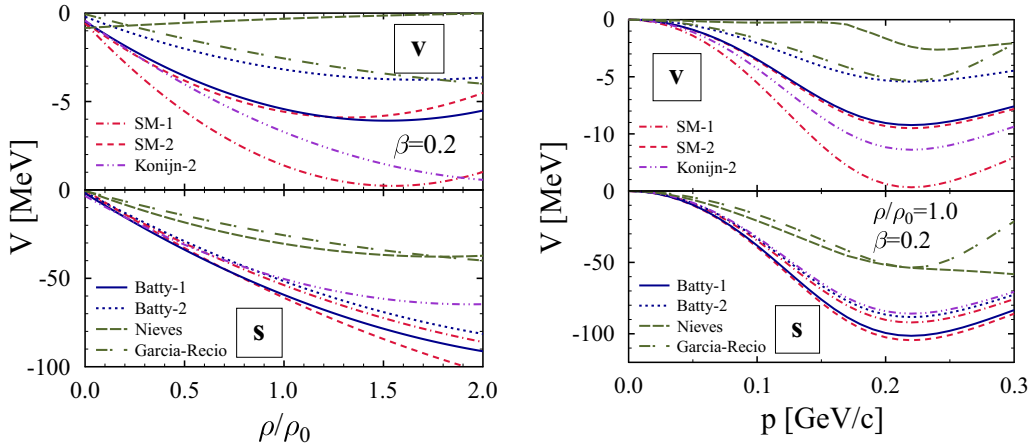

FIG. 2. The same as in Fig. 1, but for the P-wave potential. In this case the results of two theoretical models are shown, namely the one of Nieves *et al.* [43] and that of Garcia-Recio *et al.* [56]. As discussed in the text the momentum dependence of the P-wave potentials extracted from pionic atom data has been extrapolated using the momentum dependence of the latter theoretical model. The presented results correspond to the case of *uniform* nuclear matter of given density and isospin asymmetry $\beta = 0.2$. Consequently, the density gradient term that appears in Eq. (7) does not contribute.

A realistic dependence on momentum of the P-wave potential is therefore crucial, as will be shown for the observables of interest in Sec. III. The evident p^2 dependence from Eq. (7) is only valid at small pion kinetic energies and far away from the position of the pole masses of excitable baryonic resonances. This requirement is fulfilled in the case of pionic atoms. As the energy is increased and the lowest lying resonance, $\Delta(1232)$, is excited, the dependence of the pion P-wave potential on momentum is modified, influenced primarily by the energy dependence of the decay width of the resonance in question. A precise energy dependence of the potential can currently only be inferred from models that can determine the pion self-energy in nuclear matter for a wide enough kinetic energy range. In this respect, the theoretical model of Ref. [56], based on a local approximation of the delta-hole model, has allowed a good description of pion nucleus scattering up to kinetic energies of the incident pion of about 300 MeV. While more sophisticated models do exist in the literature [43], they have a limited range of applicability (pion kinetic energy $\omega \leqslant 50$ MeV) and consequently present an (unrealistic) increase in strength with ω even for invariant mass values above the position of the $\Delta(1232)$ resonance. Extrapolations of such a potential, above its range of applicability, by using three-level type models for the pion-self energy in nuclear matter, as the one proposed in Ref. [70], and used recently in [71], are considered here also inaccurate since the width of the $\Delta(1232)$, not just its energy dependence, is completely neglected in these cases. The energy dependence of the P-wave potential derived in Ref. [56] is adopted in this study. In practice, this is achieved by multiplying the P-wave part of the potential of Eq. (7) by the form factor,

$$f(p^2) = \frac{1.0 - p_{\rm eff}^2/\Lambda_1^2 + p_{\rm eff}^4/\Lambda_2^4}{1.0 - p^2/\Lambda_1^2 + p^4/\Lambda_2^4}, \qquad (13)$$

with $\Lambda_1 = 0.55$ GeV and $\Lambda_2 = 0.22$ GeV. The expression in the numerator ensures that for a value of the pion momentum equal to that of the average one in a $2p$ state of a heavy pionic atom ($p_{\rm eff} = 0.05$ GeV) the strength of the potential as extracted from pionic atom measurements is reproduced. In Sec. III, in order to test the sensitivity of the observables to various isoscalar and isovector strengths of the P-wave potential, results will be presented for all potentials listed in Table II and also for the potential of Nieves *et al.* [43].

The momentum dependence of the pion P-wave potentials of Table II and of the theoretical models of Nieves *et al.* [43] and Garcia-Recio [56] is depicted in the right panel of Fig. 2 for the isoscalar (s) and isovector (v) components separately. The features described in the previous paragraph are readily observable and, as in the case of the density dependence, the theoretical models exhibit weaker attraction than the empirical ones.

Due to the dependence of the density and isospin asymmetry parameters on the spatial coordinates, the gradient operator in Eq. (7) leads, besides the term proportional to p^2, also to terms in the potential proportional to $\vec{p}\cdot\vec{\nabla}\rho$ and $\vec{p}\cdot\vec{\nabla}\beta$. They can in principle be of relevance in the study of pionic atoms [19] since in this case the pion probes mostly the region close to the surface of the nucleus. Theoretical investigations on this topic make use of density profiles of nuclei that lead to constant isospin asymmetry [36,49] within the nucleus and consequently the isospin asymmetry gradient term does not contribute. In order to be consistent with the studies that have lead to the pion potentials of Table II terms in the potential proportional to $\vec{p}\cdot\vec{\nabla}\beta$ will be neglected in the following, keeping however those proportional to the density gradient.

Their relevance can be inferred from Fig. 3, in which the ratio of the strengths of density gradient terms in the potential and of the p^2 term of the P-wave potential as a function of momentum of the pion, for several choices of the P-wave potential parameter set and a modulus of the radius vector for which the density gradient is maximum, are presented. The calculations have been performed for the case of a ^{197}Au nucleus with the density profile as specified in the caption of Fig. 3 and outward radial pion momentum orientation. Results

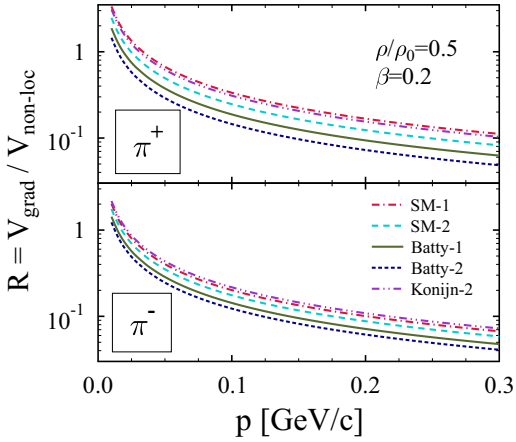

FIG. 3. Ratio R of the density gradient component of the P-wave pion potential ($V_{\rm grad}$) vs the component proportional to p^2 ($V_{\rm non\text{-}loc}$) for the π^- (bottom) and π^+ (top) mesons. Results for various choices of the P-wave potential parameter set (see Table II) are presented. The calculation has been performed for a ^{197}Au nucleus whose density profile can be parametrized by the simple expression $\rho(r) = \rho_0/\{1+\exp[(r-R)/a]\}$, with $\rho_0 = 0.165$ fm^{-3}, $R = 6.40$ fm, and $a = 0.60$ fm. The value of the coordinate r is chosen such as to maximize the magnitude of the density gradient, which for the chosen parametrization occurs at the location at which $\rho = \rho_0/2$ and hence $r = R$. The spread of the results for the chosen parameters sets of the P-wave potential is essentially given by the variation of the magnitude of ImC_0 between the different potentials.

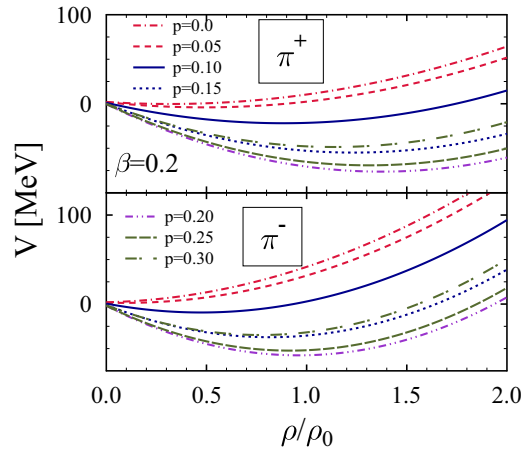

FIG. 4. Total π^- (lower panel) and π^+ (upper panel) potentials in *uniform* nuclear matter of isospin asymmetry $\beta = 0.2$ for several values of the pion momentum (expressed in GeV/c). The chiral perturbation theory inspired effective model was chosen for the S-wave part, while for the P-wave part the potential labeled Batty-1 in Table II has been selected. The other possible combinations yield qualitatively the same behavior. The repulsion generated by the density dependence of the S-wave isovector strength $\bar{b}_1$ overcomes eventually the attraction in the P-wave channel leading to a transition from a net attractive to a net repulsive potential for ever-increasing, with the pion momentum, values of the density.

for the π^- and π^+ mesons are presented in the bottom and top panels, respectively. It is readily observed that in both cases the relative strength of the gradient term potential is stronger at lower momenta, where it becomes the dominant contribution to the total pion P-wave potential. At higher momenta this relative contribution decreases to about or even below 10%. Additionally, a variation of the relative strength of the density gradient term within a factor of 2 between the different choices for the P-wave potential is observed, which can be predominantly linked to the value of the ImC_0 parameter (see Table II), which sets the strength of the two-body pion absorption processes. In the case of heavy-ion collisions, density gradients of comparable magnitude with the ones encountered in the skin of nuclei are produced over a wider range of density values. It is thus mandatory to investigate the impact of the density gradient term of the P-wave potential on pionic observables.

This section is concluded by presenting, in Fig. 4, the π^- (bottom panel) and π^+ (top panel) total S+P pion potential in uniform nuclear matter as a function of density for various values of the pion momentum p. The effective model is chosen for the S-wave part and the Batty-1 parameter set of Table II for the P-wave component. The total potential is repulsive for small values of the pion momentum irrespective of density. At higher momenta, the potential becomes attractive; however, as the density increases, the repulsive S-wave part prevails resulting again in a net repulsive interaction. Due to the isovector component, the potentials of the π^- and π^+, while showing qualitative similarities, differ in strength by non-negligible amounts with foreseeable impact on isovector observables.

III. PION POTENTIAL AND PION OBSERVABLES

The impact that the small modifications to the transport model, as described in Sec. II A, have on the PMR is presented in Fig. 5. A comparison between the PMR in central ^{197}Au +^{197}Au central collisions at an impact energy

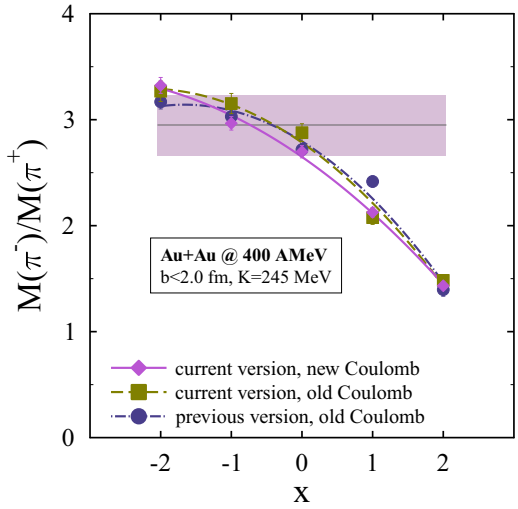

FIG. 5. Impact of the modifications of the model described in Sec. II A on the multiplicity ratio of π^- and π^+ mesons as compared with the result of Ref. [15]. The ordinate x parametrizes the stiffness of the symmetry energy, negative and positive values corresponding to a stiff and a soft asy-EOS, respectively. The horizontal band depicts the experimental result of the FOPI Collaboration [21].

of 400 MeV/nucleon for the case of the previous version of the model [15] (dashed-dotted curve) and the current one when first the corrected expression of Eq. (4) for rms is used (dashed curve), and then also the strength of the Coulomb is adjusted to match its contribution to the binding energy as provided by the empirical nuclear mass formula (full curve), as described in Sec. II A, is presented. For each of the calculations presented the GEC scenario has been adopted, the isovector $\Delta(1232)$ potential strength has been set to $V_v = \delta$, and the pion potential has been switched off. The rest of the model parameters are set to values as described in Sec. II A. The extracted value of the SE stiffness is only marginally impacted by the correction to the rms formula. On the other hand, the modification of the strength of the Coulomb interaction leads to a stiffer asy-EOS, the increase of the extracted slope L of SE being of the order of 15 MeV (see Table I for the connection between x and L). This is comparable with the precision with which this parameter is extracted from the most recent elliptical flow results of the ASYEOS Collaboration [72].

The study reported in Ref. [15] has demonstrated that the ratio of charged pion multiplicity is equally sensitive to both the stiffness of the SE and the strength of the isovector $\Delta(1232)$ potential in nuclear matter. Consequently, constraints for the slope L of the SE at saturation cannot be extracted unambiguously without a proper knowledge of the latter. The only solution out of this problem, given that no information about the isovector $\Delta(1232)$ potential is available from either theory or experiment, is to enlarge the set of observables from which the unknown parameters of the model are extracted. Obvious candidates are the average final momenta (or kinetic energies) of charged pions. To isolate the isovector signal, similarly to the case of multiplicities, it will prove useful to construct their ratio. In addition to multiplicities, the FOPI experiment has also measured the final transverse momenta of pions and results for the ratio of average p_T of π^+ and π^- are available in the literature for several systems and impact kinetic energy equal to or higher than 400 MeV/nucleon [20]. Consequently, results and comparisons with available experimental data [20,22], for average transverse momenta of pions and their ratio, will also be presented, where considered useful.

The impact that the various energy conservation scenarios, introduced in Ref. [15] and briefly described in Sec. II A, has on average p_T of pions and their ratio is presented in Fig. 6. Its left-hand panel presents the impact of the VEC, LEC, and GEC scenarios on the pion average p_T ratio (PAPTR). VEC and GEC scenario simulations reveal values of PAPTR that overshoot the experimental FOPI result [20] by 10%–20%. On the other hand the LEC scenario leads to PAPTR values below their experimental counterpart by at most 10%. The impact of local energy conservation (as compared to VEC) is therefore much more pronounced for PAPTR than for multiplicity ratios, while the difference between LEC and GEC scenarios is equally dramatic for these two observables. Decreasing the strength of the Coulomb interaction by 10% (previous vs current versions of the model) results in a reduction, in agreement with expectations, of the PAPTR by about 5%. A moderate dependence of PAPTR on the SE stiffness is also demonstrated, a softer asy-EOS leading to a higher PAPTR for the VEC and GEC scenarios and the opposite for LEC.

The right-hand panel of Fig. 6 gives the sensitivity of the average transverse momenta of each of the three charge pion states to the selected energy conservation scenario. It is shown that the low value of PAPTR in the case of the LEC scenario originates predominantly from the impact the local conservation of energy (LEC) has on the average transverse momentum of the π^- meson. The same holds true for the origin of the differences between the VEC and GEC scenarios and the

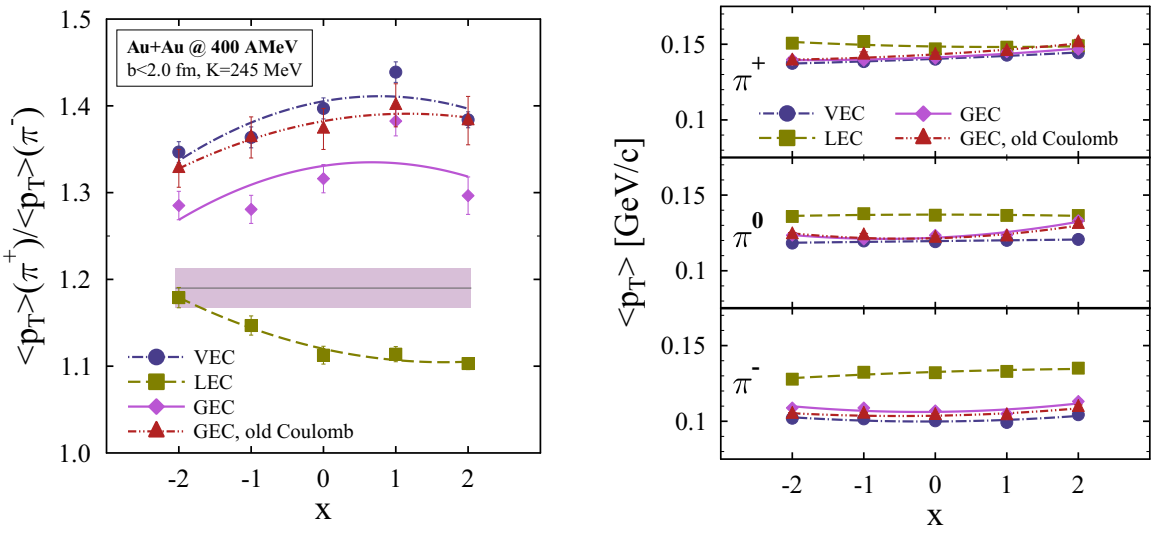

FIG. 6. Average p_T ratio of charged pions (left panel) and average p_T of all charge states of the π meson (right panel) as a function of the stiffness parameter x in central ^{197}Au $+^{197}$Au collision at an impact energy of 400 MeV/nucleon. Results for the VEC (dashed-dotted curves), LEC (dashed curves), and GEC scenarios are presented. For the case of the GEC scenario results for two strengths of the Coulomb interaction are shown: the one of Ref. [15] (dashed-double-dotted curves) and the one used in this study (full curves). The FOPI experimental result for the PAPTR [20] is depicted by a horizontal band.

modification on PAPTR induced by changing the strength of the Coulomb interaction, even though in this case the changes are much smaller in magnitude. These observations are on par with the impact of the energy conservation scenarios on pion multiplicities [15].

The results of the attempt to explain the remaining difference between the GEC result for PAPTR and its experimental value by including the effect of the pion-nucleus potential will be presented in the following. Since experimental values for pion average transverse momenta were available only for mid-central collisions (3.35 fm $< b <$ 6.0 fm) [22] the study of the impact of pion potentials on pion observables has been performed for this impact parameter range. To allow a comparison with the experimental data, the following kinematical filter has been applied to theoretical data: $p_T <$ 0.33 GeV/c and $|y| < 1.75$. Constraints on the symmetry energy stiffness will however be extracted from published central collision data ($b <$ 2.0 fm), since only for this case systematical uncertainties have been included in the estimation of total uncertainties of experimental data.

The impact of the S-wave potential on pion multiplicities and average transverse momenta is presented in Fig. 7. The case when contributions of the pion potential are omitted is presented as a benchmark. The impact on multiplicities (left-hand panel) is stronger for the case of π^- and generally an S-wave potential that is stronger at saturation densities and above leads to a stronger decrease of the multiplicity in question. The most clearly visible example is that of the Konijn-2 potential. The weaker SM-1 and Nieves *et al.* potentials lead to the smallest change with respect to the no pion potential case. Additionally, accounting for the empirical momentum dependence of the S-wave isoscalar strength is also observed to impact only slightly pion multiplicities. Generally, the experimental value of charged pion multiplicities is underestimated by the model by fractions that show a weak isospin dependence.

The right-hand panel of Fig. 7 presents the conclusions on the impact of the S-wave potential on the average transverse momenta of charged pions. The cases of π^- and π^+ mesons are clearly different. In the case of negatively charged pions the impact always leads to higher average transverse momenta, the strength of the modification being, similarly to pion multiplicities, in close correlation to the strength of the potential close to saturation density. Inclusion of S-wave potential leads predominantly to values that overestimate the experimental FOPI value by at most 10%. In the case of the positively charged pions the sign of the effect of the S-wave potential on average p_T varies with the chosen potential, but in all cases the experimental values are overpredicted by amounts in the range 5%–20%. For the case of the theoretical potential of Nieves *et al.* the impact is again among the smallest for both charged pion states. The impact of the momentum dependence part of the potential on transverse momenta is however clearly visible, leading to increases of these observables by 5%–10%.

The impact of the P-wave potential is presented in Fig. 8. In all cases presented in this figure the momentum-dependent effective S-wave potential describe in Sec. II B and summarized in the paragraph adjacent to Eq. (12) has also been included, allowing a comparison of the full model with the experimental data. From the left-hand panel of this figure the impact of the P-wave potential on multiplicities can be inferred. For both charged states it stays below 10%, but is in relative magnitude bigger for the positively charged pion. The impact of the density gradient term of the potential is visible particularly for the π^+ meson leading to an increase of a few percent of its multiplicity.

The impact of the P-wave pion potential on average p_T values is clearly more important as can be seen from the

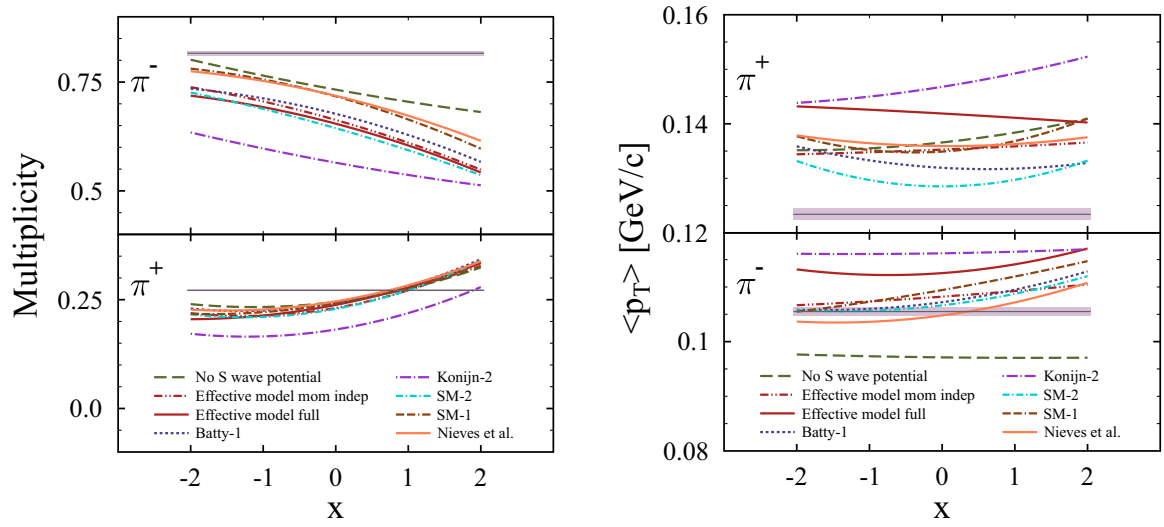

FIG. 7. Impact of the S-wave pion potential on pion multiplicities (left panel) and pion average transverse momenta (right panel) in mid-central collisions (3.35 fm $< b <$ 6.00 fm) of ^{197}Au $+^{197}$Au at an incident energy of 400 MeV/nucleon for various choices of the S-wave potential, as presented in Sec. II B. The following kinematical cuts have been applied: $p_T <$ 0.33 GeV/c and $|y| < 1.75$. The curves labeled "No S-wave potential" were obtained by omitting any contributions due to the pion optical potential. Experimental data [22] are represented by horizontal bands, with their widths representing only the statistical uncertainties (systematic uncertainties were not available).

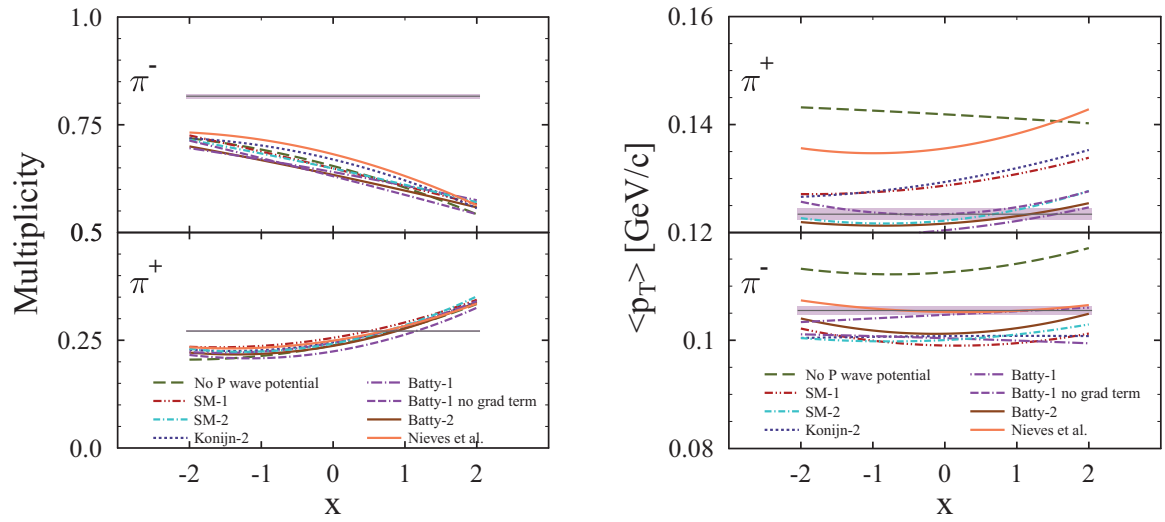

FIG. 8. Impact of the P-wave pion potential on pion multiplicities (left panel) and pion average transverse momenta (right panel) in mid-central collisions (3.35 fm $< b <$ 6.00 fm) of ^{197}Au $+^{197}$Au at an incident energy of 400 MeV/nucleon for various choices of the P-wave potential, as presented in Sec. II B. The following kinematical cuts have been applied: $p_T < 0.33$ GeV/c and $|y| < 1.75$. The calculations labeled "No P-wave potential" include the impact of the effective model S-wave pion potential alone. The same remark for the experimental values (horizontal bands), as the one made in the caption of Fig. 7, holds true.

right-hand panel of Fig. 8. Its attractive nature leads to lower values of p_T for all presented choices for the P-wave potential, the relative impact amounting to as much as 15%. Generally, the experimental values of the π^- and π^+ transverse momenta cannot be described simultaneously. This suggests that the isovector part of the pion potential, as included in the present model, is not accurate enough, either in strength or density dependence. Additionally the density gradient term of the P-wave potential is seen to have a discernible effect, at a few percent level, for both shown charge states of the π meson. This result leads one to speculate on the possible relevance of the omitted isospin asymmetry gradient term in the P-wave potential.

It is noteworthy to investigate separately the impact of pion potentials on the observables of primary interest for constraining the density dependence of the symmetry energy. To this end the influence of the S- and P-wave potentials on PMR and PAPTR in mid-central collisions of ^{197}Au $+^{197}$Au nuclei at 400 MeV/nucleon impact energy are presented in the left-hand and right-hand panels of Fig. 9, respectively. They are obviously derived from the information presented in previous figures.

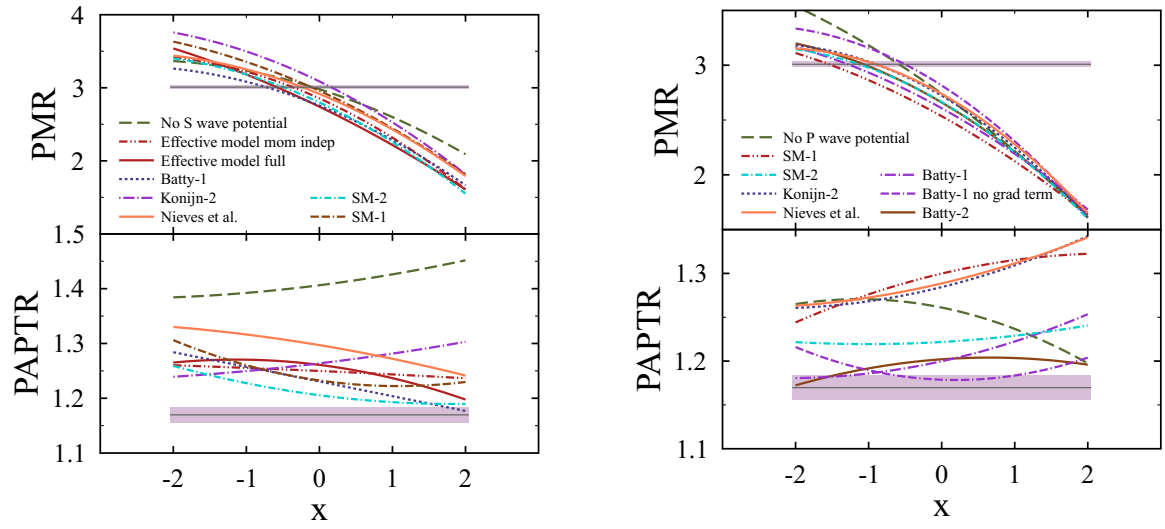

FIG. 9. Impact of the various S (left panel) and P (right panel) wave pion potentials introduced in Sec. II B on pion multiplicity ratio (PMR) and pion average p_T ratio (PAPTR) in mid-central collisions (3.35 fm $< b <$ 6.00 fm) of ^{197}Au $+^{197}$Au at an incident energy of 400 MeV/nucleon. The meaning of the curves labeled "No S-wave potential" and "No P-wave potential" is the same as in Figs. 7 and 8, respectively.

The inclusion of the S-wave pion potential leads in the majority of cases to a smaller PMR, the impact on the extracted slope parameter L of the SE amounting to as much as 20 MeV towards stiffer values. The momentum dependence of its isoscalar component influences the PMR only modestly. A similar conclusion holds also for the P-wave pion potential impact; the value of the PMR is further reduced, pushing the extracted stiffness of the asy-EOS to even higher values. From the right-hand panel of Fig. 9 an estimated impact of 20–40 MeV is obtained. It is noteworthy to point out that the influence of the density gradient term is important, pushing the PMR to lower values. Most of the impact of the P-wave pion potential on PMR is due to its gradient term. The combined effect of the S- and P-wave pion potential is to lower the PMR and consequently push the extracted values of L towards higher values by as much as 40–60 MeV. This margin is comparable to the precision achieved in constraining the slope of the symmetry energy at saturation using elliptical flow data of the FOPI-LAND collaboration [31,32,73], but a factor 2–3 larger than the foreseeable accuracy that will be reported in the near future using the experimental results for the same observable measured by the ASYEOS Collaboration [72].

Turning to PAPTR, it is readily observed that the inclusion of the S-wave pion potential leads, for all presented choices of the potential, to smaller values of this observable. The model generally leads to values of this observable higher than the experimental one, the discrepancy growing larger towards stiffer values of L. As in the case of the PMR, the impact of the momentum-dependent part of the isoscalar part of the S-wave pion potential is small. The sign of the contribution of the P-wave potentials to the final value of the PAPTR varies with the chosen potential. Only a few of the P-wave potentials used in this study were able to lead to values of the PAPTR in agreement or close to its experimental one. It should however be noted that for the study of impact of the P-wave potential the included S-wave component was that of the so-called "full effective model" which can be observed, from the left panel of Fig. 9, to lead to higher values of PAPTR than some S-wave potentials extracted from pionic atom data. The impact of the density gradient term of the P-wave potentials is at the level of a few percent and leads to lower and higher value of PAPTR for the a stiff and soft asy-EOS, respectively. Furthermore the direction of the impact (increase vs decrease) was revealed to be, during this investigation, dependent also on the choice of the P-wave potential. It can be concluded that for an accurate description of the experimental value of PAPTR both the S- and P-wave pion potentials need to be precisely known from other sources if models that take into consideration particle production threshold effects and enforce the conservation of the total energy are employed.

A comparison of predictions of the full model with experimental rapidity and transverse momentum spectra of pions [22] will be postponed until the end of next section, in order to be able to make use of the extracted strength, from experimental data, of the isovector $\Delta(1232)$ potential.

This section is concluded with a presentation, in Fig. 10, of the time evolution of the average transverse momenta of the three charge states of the pion during heavy-ion collisions. Four cases have been selected for this study. For the first one the effect of pion potentials is completely neglected (labeled "no pion pot"). The other three are obtained by successively adding the following ingredients to the first case: the S-wave pion potential ("S-wave"), non-density-gradient terms of the P-wave pion potential ["S+P (non-grad)"], and the density gradient term of the P-wave potential ["S+P (full)"]. The addition of each of these contributions leads to important modifications of the average p_T of pions at earlier stages of the collision, particularly during the high-density phase. The impact of the S- and P-wave components of the potential are of comparable magnitude; there is however a noticeable isospin dependence for the former one. The influence of the gradient terms of the P-wave potentials on the final values of transverse momenta is smallest, at a few percent level. It is however clear that the outcome of the full model is the result of fine (partial) cancellations of the effects of all the components of the pion potential, making the need for their precise knowledge more transparent.

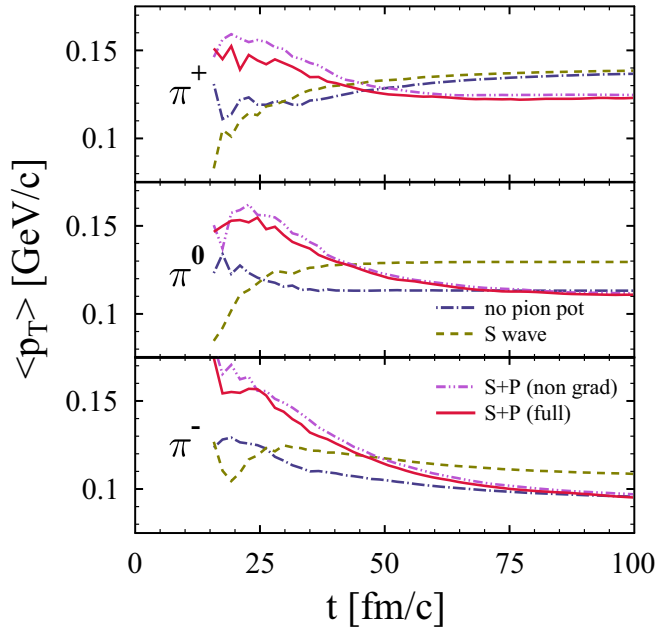

FIG. 10. Time dependence of the average transverse momentum of π^- (top), π^0 (middle), and π^+ (bottom) mesons in mid-central heavy-ion collisions of ^{197}Au + ^{197}Au at an incident energy of 400 MeV/nucleon for several choices for the total potential experienced by pions besides Coulomb. The value of the stiffness parameter has been set to $x = 0$ and the Batty-1 parametrization of the P-wave pion potential has been selected where indicated. The labels bear the following meaning: "no pion pot", both components of the pion potential have been omitted; "S-wave", only the effective model S-wave pion potential has been included; "S+P (non-grad)", the S-wave and nongradient terms of the P-wave potential have been included; and finally "S+P (full)", the S wave and the full P wave (both the gradient and nongradient terms) are taken into account. The vast majority of the pions that escape into detectors are emitted at moments ulterior to $t = 30$ fm/c.

IV. CONSTRAINING THE SYMMETRY ENERGY

Given the modifications of the transport model described in Sec. II A and the inclusion of the pion optical potential

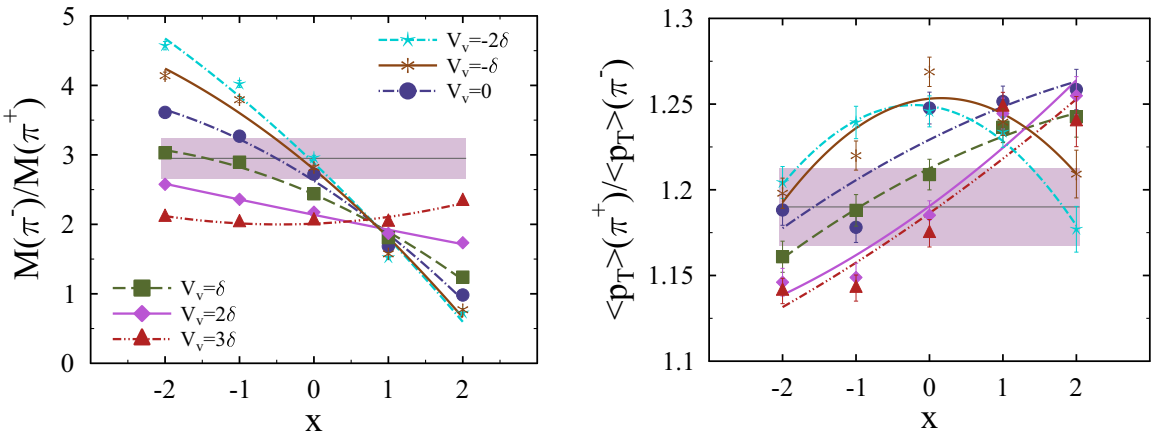

FIG. 11. The ratio of charged pion multiplicities (left panel) and average transverse momenta (right panel) as a function of the stiffness parameter x for six different choices of the strength of the isovector component of the $\Delta(1232)$ potential in nuclear matter [see Eq. (6)]. The results correspond to central ($b < 2.0$ fm) ^{197}Au $+^{197}$Au collisions. The full experimental FOPI results (including both systematical and statistical errors) of Refs. [20,21] are depicted by horizontal bands.

it is worthwhile to rediscuss the impact of the $\Delta(1232)$ isovector potential on the PMR and stress the differences with the conclusions of the initial investigation reported in Ref. [15]. The analysis will be extended to include the PAPTR and also to a wider range of the strength of the isovector $\Delta(1232)$ potential. The latter quantity will be allowed both attractive and repulsive strengths in the range $[-2,3]$ in units of δ [see Eq. (6) and the paragraph following it]. The effects due to the effective model for the S-wave pion potential and Batty-1 parametrization for the P-wave one (with an energy dependence as discussed in Sec. II B) have been included. The results of this simulation are presented in Fig. 11.

The impact of the strength of the isovector $\Delta(1232)$ potential on the PMR is presented in the left-hand panel of Fig. 11 for different values of the asy-EOS stiffness parameter x. The strong dependence of the PMR on this quantity for all values of x, with the exception of a narrow interval that encloses $x = 1$, is evident. The sensitivity decreases however for attractive choices of the strength V_v and becomes rather small in the neighborhood of $V_v = -2\delta$. As already noted at the beginning of Sec. III, the small changes implemented to the transport model, with respect to Ref. [15], lead to a slightly lower value for PMR and somewhat modified dependence on x, mostly due to the decrease of the strength of the Coulomb interaction. This is most easily visible for the strength of the isovector $\Delta(1232)$ potential $V_v = 3\delta$. For this case the current model leads to PMR values that are largely independent of x, while the version of Ref. [15] gives rise to increasing PMRs with increasing SE softness allowing the description of the experimental FOPI value for a very soft asy-EOS. Extrapolations of the presented results suggest that the current model would be able to describe the experimental PMR data for a stronger than $V_v = 3\delta$ isovector $\Delta(1232)$ potential and a soft SE, in addition to the cases evident from the left panel of Fig. 11.

The right-hand panel of Fig. 11 presents the dependence of the PAPTR on both the strength of the isovector $\Delta(1232)$ potential and the SE stiffness parameter x. By fixing the former it can be concluded that the PAPTR is sensitive to the isovector part of the EOS. The sensitivity to its stiffness is however considerably less pronounced than for PMRs, amounting to at most 10% between the very soft and very stiff choices for x. This feature is more clearly visible for repulsive values of V_v and in particular for the choice commonly employed in most transport models $V_v = \delta$. For attractive V_v the sensitivity to the SE decreases to about 5%, but for these cases the theoretical PAPTR values tend to overpredict the experimental one. With regard to the extraction of constraints for the SE stiffness it should be noted that experimental values for this observable are determined with much higher accuracy than for PMR (2.5% vs 10%) which balances to a certain extent the disadvantage of a lower sensitivity to the asy-EOS stiffness. The sensitivity of the PAPTR to V_v mirrors almost perfectly the behavior evidenced for the PMR. It reaches a maximum for stiff choices of the asy-EOS and becomes smaller for soft ones, vanishing in the neighborhood of $x = 1$.

It is instructive to present the comparison theory versus experiment as χ^2/dof plots for the observables of interest that also exhibit the above discussed sensitivity to the stiffness of the symmetry energy and strength of the $\Delta(1232)$ isovector potential. This is achieved in the left panel of Fig. 12 for the PMR. To facilitate the extraction of information about the favored value of x (and V_v) curves for the 68%, 95.5%, 99.3%, and 99.994% confidence levels, which allow the determination of 1, 2, 3, and 4σ uncertainties on the extracted value of the desired parameter, are plotted. They are labeled by the corresponding value of χ^2/dof. The conclusions of Ref. [15], which can also be inferred from the left panel of Fig. 11, with regard to suitability of the PMR for the extraction of constraints for the density dependence of SE above saturation are more transparent. Specifically, the extracted value for x depends strongly on V_v and, furthermore, for a repulsive isovector $\Delta(1232)$ potential the uncertainty increases as a result of the lower sensitivity of PMR to the asy-EOS stiffness. In contrast, for the hypothetical case of an attractive isovector

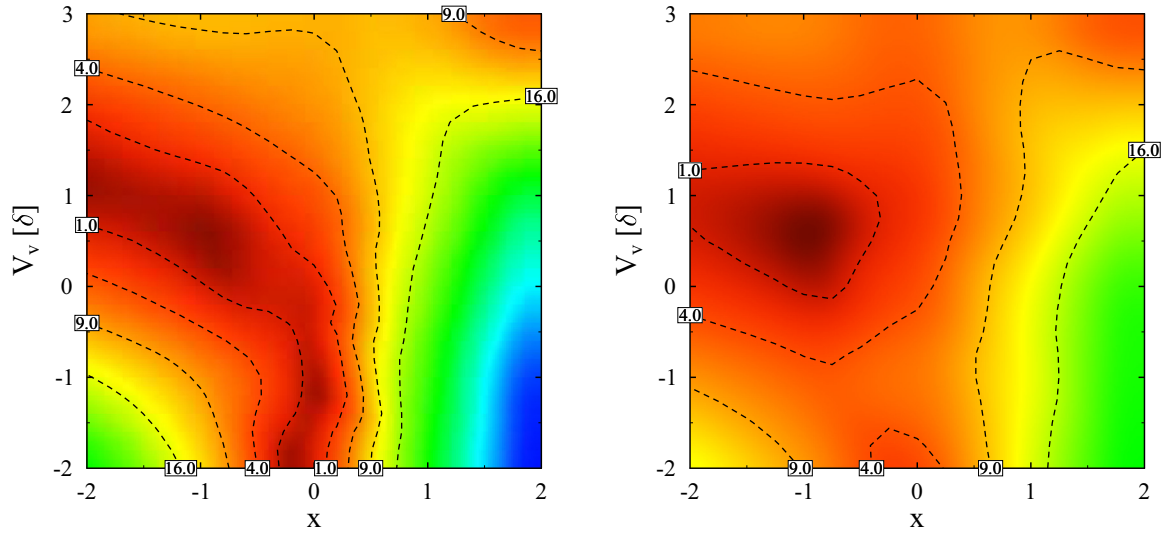

FIG. 12. Contour plots for the χ^2/dof value of the comparison theory vs experiment for the case of the PMR (left panel) and PMR+PAPTR (right panel). In the latter case, contributions due to the two observables are added with the same weights. Curves are labeled according to the corresponding value of the χ^2/dof quantity.

$\Delta(1232)$ potential the stiffness of the SE can be more accurately determined and is almost independent of the value of V_v.

The observed impass can be resolved by including in the expression of χ^2/dof contributions due to PAPTR. This claim is supported by the results presented in the right-hand plot of Fig. 12. It is observed that the range of allowed, at 1σ confidence level, isovector $\Delta(1232)$ potential strength values V_v is significantly narrower, favoring a mildly repulsive one, as compared to the case when only contribution due to PMR are included. Similarly, the allowed range for the stiffness parameter x is more constrained at 1σ level to $x = -1.0^{+0.75}_{-1.5}$. The corresponding value for the allowed slope parameter interval is $L = 106^{+67}_{-34}$ MeV. The accuracy is comparable with the one that can be achieved from elliptic flow ratio constraints that make use of the FOPI-LAND experimental data [31,32,73], but is a factor of 2–3 more imprecise than what can be accomplished by using the most recent ASYEOS Collaboration results for similar observables [72]. The less than optimal accuracy when extracting the value of L from pion-related observables originates from three main sources: first, the sensitivity of the PMR to the SE stiffness decreases towards higher values of L; second, the experimental uncertainty on PMR amounts to a rather large value, close to 10%; third, the sensitivity of PAPTR to the slope parameter L is not as pronounced as for the PMR.

Each of these three sources of uncertainties can be reduced in the following manner: (1) choosing nuclei with higher isospin asymmetry; (2) performing experimental measurements at lower impact energies, closer or even below the vacuum pion production threshold; and (3) improving experimental accuracy. All of these requirements will be fulfilled by measurements that will be performed in the very near future by the SAMURAI TPC collaboration [74]. For the already existing FOPI experimental data only the last source can be partially alleviated by performing a reanalysis of the available data sets and excluding from the spectra the regions of increased systematic uncertainties, as is for example the low-energy part of the pion spectrum.

Before such an improved experimental result will become available, it will be useful to attempt to estimate the impact of such an effort on the extracted constraints for the slope parameter L and isovector $\Delta(1232)$ potential strength V_v. This exercise will also offer indications about the potential of the experimental program put forward by the SAMURAI TPC collaboration [74]. To this end, the uncertainties of the experimental FOPI values for the PMR and PAPTR in central ^{197}Au+^{197}Au collisions at an impact energy of 400 MeV/nucleon have been decreased artificially from 9.5% to 3% and from 2.5% to 1.5%, respectively. The results are plotted in the right-hand panel of Fig. 13 for the case when the Batty-1 P-wave pion potential is used by the double-dashed-double-dotted curve (labeled "Batty-1 low exp err"). The case when the full magnitude of the experimental uncertainties is considered is depicted by the full curve (labeled "Batty-1"). The important "improvement" of the experimental accuracy leads to an increase of the accuracy of the extracted values for L and V_v by a fraction amounting to about 30%–40% of the old result. It can thus be concluded that a precise determination of the slope parameter from pion observables will require a very careful choice of the system studied and of the impact energy together with a significant improvement of the experimental accuracy to values in the few percent range.

The success of such a program will only be warranted if certain progress on the theoretical side, mainly a better knowledge of the pion potential away from the density and kinetic energy region that was constrained using pionic atoms and pion-nucleus scattering, will be also achieved. To support this statement, the 1σ confidence level (CL), if not otherwise specified, of the theoretical versus experimental comparison of PMR+PAPTR has been plotted in Fig. 13 for

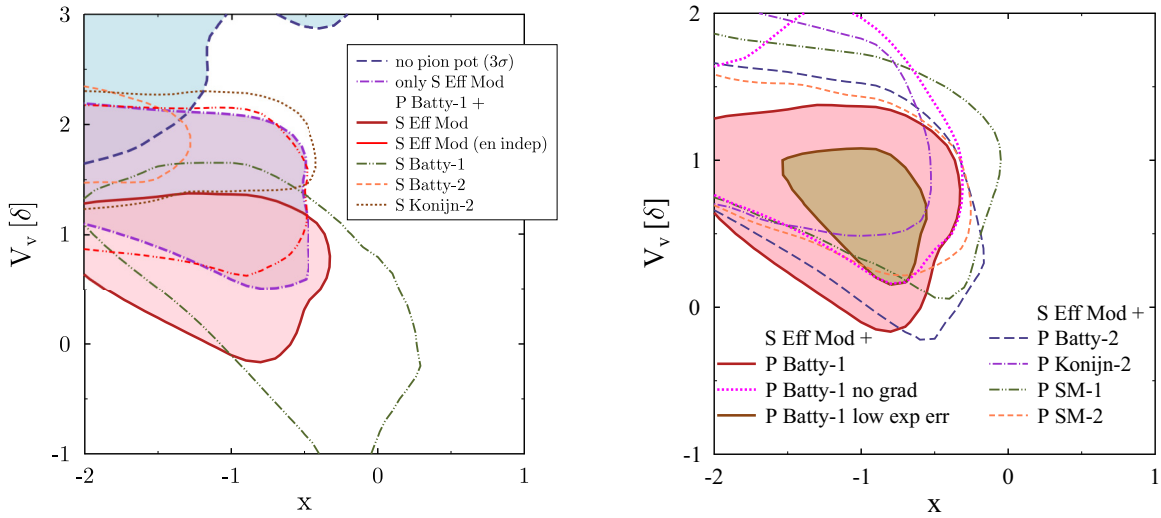

FIG. 13. Sensitivity of the extracted constraints for the stiffness parameter x and strength of the isovector $\Delta(1232)$ potential V_v to different choices for the S-wave (left panel) and P-wave (right panel) pion potentials. The calculations help quantify the impact of uncertainties in the energy and density dependence of these potentials on the quantities of interest. For that purpose the 1σ confidence level (CL) contour plots of the quantity χ^2/dof determined by comparing theoretical and experimental results for the observables PMR and PAPTR for different choices for the pion S-wave (left panel) or P-wave (right panel) potentials are plotted. The case for which pion potential contributions are completely omitted ("no pion pot") or only the S-wave component is included ("only S Eff Mod") are also shown (left panel). Result for a version of the P-wave potential with the gradient terms omitted is also shown ("P Batty-1 no grad" in the right panel). Additionally, for the Batty-1 parametrization of the P-wave potential the 1σ CL contour curve determined by artificially decreasing the experimental uncertainties for PMR and PAPTR to 3% and 1.5%, respectively, is also plotted and labeled "P Batty-1 low exp err" (right panel).

various choices of the pion S-wave (left panel) and P-wave (right panel) potential, while keeping the other component (P-wave for the left panel and S-wave for the right panel) the same. Such calculations help quantify the model dependence introduced by extrapolating the pion potential far outside the density/momentum region probed in pionic atom and pion-nucleus scattering experiments.

A calculation in which both pion potential components have been omitted has also performed and it demonstrates that a simultaneous description of the experimental values for PMR and PAPTR cannot be achieved for any reasonable choices of the x and V_v parameter values. In fact, most of the probed parameter space lies outside the 3σ CL region (see the dashed curve and the filled region enclosed by it in the left panel of Fig. 13). The inclusion of the S-wave potential, with the P-wave potential switched off ("only S Eff Mod"), drastically improves the situation, the 1σ CL region being almost entirely inside the parameter search window. Switching on the P-wave potential ("P Batty-1 + S Eff Mod") impacts visibly only the favored value of V_v, the extracted value for the stiffness parameter x being virtually the same. A similar conclusion holds true in regard to the impact of the energy-dependent piece of the S-wave potential (compare double-dashed-double-dotted and full curves in the left panel of Fig. 13). Different density dependencies for both the isoscalar and isovector parts of the S-wave pion potential do however have an important impact on the extracted values of both x and V_v parameters. The uncertainty of the favored value for the slope L can amount to as much as 60 MeV. In this context it should be recalled that all the employed S-wave potentials have very similar strengths in the $0.5\rho_0$–$0.75\rho_0$ density region, but they differ significantly above saturation in either the isoscalar or the isovector channel (see left panel of Fig. 1).

The magnitude of the model dependence due to uncertainties in the P-wave pion potential can be inferred from the right panel of Fig. 13. Results for each of the parametrizations listed in Table II are provided. It can be seen that the minimum allowed value for L varies rather strongly with the choice of the potential between the limits $L = 61$ MeV ($x = 0.0$) and $L = 85$ MeV ($x = -0.5$). Furthermore, for all of the used P-wave potentials the maximum value of L satisfies the constraint $L > 150$ MeV. Additionally, the impact of the gradient terms of the P-wave potential can be assessed by comparing the full and dotted curves in the same plot. It is seen that they affect visibly only the extracted value of the V_v parameter.

Taking into account all evidenced sources of uncertainty one can deduce, from a comparison of the present model and the available experimental FOPI data for PMR and PAPTR, that at 68% CL the slope of the symmetry energy at saturation has to be stiffer than $L = 50$ MeV irrespective of the strength of the $\Delta(1232)$ potential or of details of the pion optical potential. This lower limit is further decreased to roughly $L = 30$ MeV and $L = 15$ MeV to achieve a 95.5% and 99.3% CL result. It can be therefore concluded, with sufficient certainty, that the density dependence of the symmetry energy is not soft. The extraction of an upper limit with a similar confidence level will have to be postponed until more precise data of a reaction more sensitive to the density dependence of the SE become available.

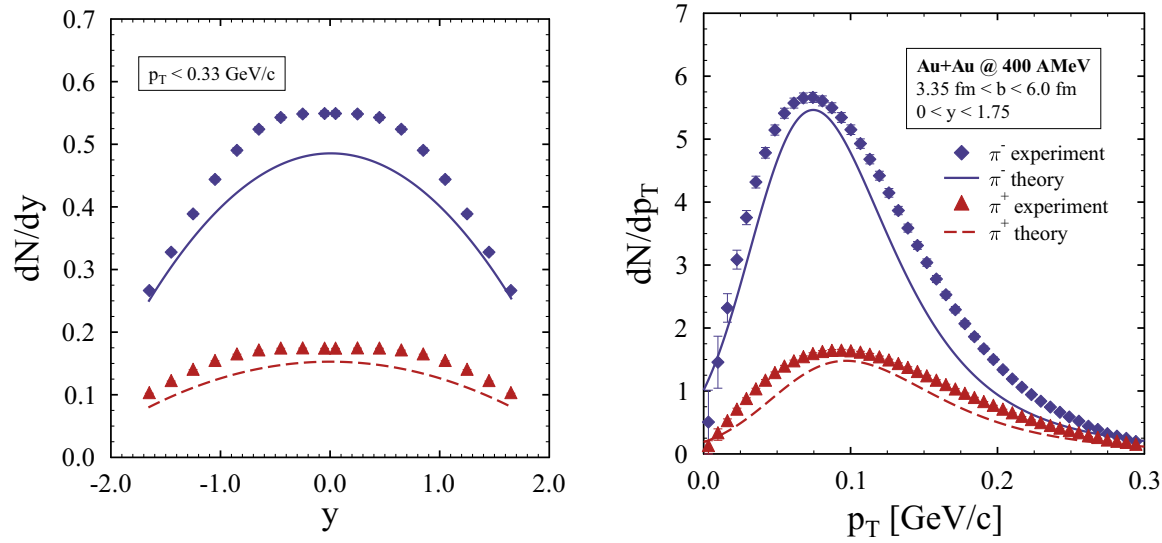

FIG. 14. Rapidity (left-hand panel) and transverse momentum (right-hand panel) spectra of charged pions in mid-central ^{197}Au + ^{197}Au collisions at impact energy of 400 MeV/nucleon. Theoretical results for π^- (full curves) and π^+ (dashed curves) mesons are compared with their experimental counterpart [22] depicted by diamond and triangle shaped symbols, respectively. In addition to the impact parameter selection (3.35 fm $< b <$ 6.0 fm) the indicated kinematical cuts were imposed in each case. The value of the stiffness parameter has been set to $x = -1$. Systematic uncertainties were not accounted for in the plotted experimental error bars.

The present transport model favors, on average, when the Batty-1 parametrization for the P-wave potential is employed a rather soft repulsive $\Delta(1232)$ potential, with $V_v = 0.5\delta$. Using this result, the charged pion rapidity and transverse momentum spectra have been determined and are plotted in Fig. 14 together with the FOPI experimental result [22]. For this theory versus experiment comparison the value of the stiffness parameter has been set to $x = -1$, which is close to the average value favored by the model in conjunction with the Batty-1 P-wave pion potential (see Fig. 13). The comparison is performed for mid-central collisions of ^{197}Au + ^{197}Au nuclei, the additional imposed kinematical constraints being $0 < y/y_P < 1.75$ and $p_T < 0.33$ GeV/c. It is observed that both the rapidity and p_T experimental spectra are underpredicted by the model by fractions in the range of 10%–20% particularly in the mid-rapidity and higher than average p_T regions. The high-rapidity and high-p_T ends of the shown spectra are generally in close agreement to the data. As the π^- and π^+ multiplicities increase and respectively decrease with the increase of asy-EOS stiffness the observed general underprediction of experimental data for these two observable may be reduced by a fine adjustment of the isoscalar part of the mean-field potential, in particular that of the rather uncertainly known isoscalar $\Delta(1232)$ potential. The momentum dependence of the difference theory versus experiment underlines the need for a precise knowledge of the momentum-dependent part of the optical potentials the model relies upon.

The same experimental data set can be used to perform a comparison theory versus experiment for the transverse-momentum-dependent PMR. The results are presented in Fig. 15 for all five choices of the stiffness parameter x used in this study. The general feature of all the theoretical sets is that the slope of the transverse-momentum-dependent PMR is mildly stiffer than the experimental one at low and average values of p_T and moderately softer at the high-end

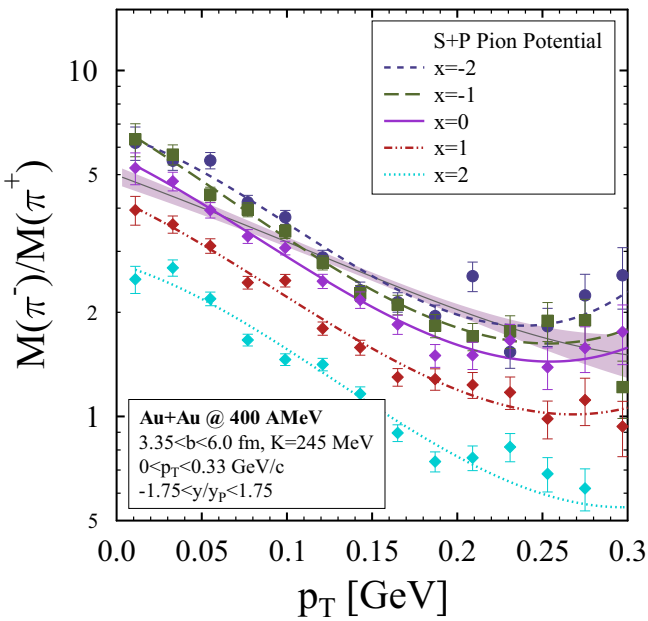

FIG. 15. Theoretical transverse momentum PMR spectra in mid-central ^{197}Au + ^{197}Au collisions at an impact energy of 400 MeV/nucleon compared to its FOPI Collaboration experimental value [22]. The effective model S-wave and the Batty-1 P-wave pion potentials have been accounted for in the simulations. Results for five values of the stiffness parameter x are plotted. Remarks made in the caption of Fig. 14 hold also for the case presented here.

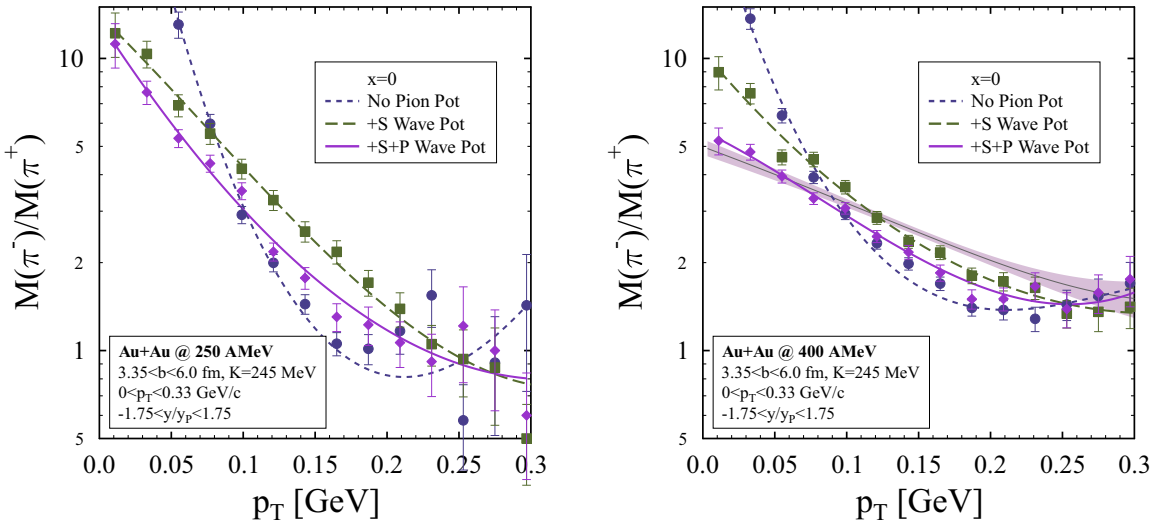

FIG. 16. The impact of the S-wave and P-wave components of the optical pion potentials on the transverse momentum PMR in mid-central ^{197}Au $+^{197}$Au collisions for two different values of the impact energy: $T_{\rm lab} = 250$ MeV/nucleon (left panel) and $T_{\rm lab} = 400$ MeV/nucleon (right panel). For the latter case the experimental FOPI result [22] is shown as a band. The value of the asy-EOS stiffness parameters has been set to $x = 0$ ($L = 61$ MeV). The same kinematical cuts as in Fig. 14 have been applied.

part. As will become evident from Fig. 16 this observable is greatly influenced by the S-wave pion potential and to a lesser extent also by the P-wave one. An accurate knowledge of the momentum-dependent parts of the two components of the pion optical potential is therefore mandatory for a successful description of the p_T-dependent PMR. It should be recalled that in this respect the approach employed in this study has been rather qualitative, due to the lack of needed knowledge in this area. For the momentum-dependent part of the S-wave pion potential a reproduction of the empirical values of the effective isoscalar scattering amplitude $\bar{b}_0^{\rm eff}$, which have been extracted from pion-nucleus scattering experiments, has been imposed. In the case of the P-wave potential, the strength extracted from pionic atom data has been extrapolated to the energy of interest by mirroring the momentum dependence of the theoretical potential of Ref. [56]. It is worth recalling that the experimental data plotted in Fig. 15 do not include systematical uncertainties and consequently the mild to moderate differences between the experimental and theoretical slopes of the p_T-dependent PMR may not be statistically significant. Besides these observations, it is evident that the experimental data are qualitatively compatible with values of the stiffness parameter $x = 0$ and $x = -1$ and to a lesser extent $x = -2$. On the other hand, soft choices of the asy-EOS stiffness, $x = 1$ and $x = 2$, underpredict the experimental values and will continue to do so also when the systematical uncertainties of the experimental data, which are of the order of 10%, will be taken into account.

The results presented in Ref. [9] have suggested that PMRs are not sensitive to the slope parameter L of the SE at saturation. It was consequently proposed that the kinetic-energy (or equivalently transverse-momentum) dependent PMR, particularly its high-energy tail, should be used in order to constraint L from experimental data. The model employed in that study included a momentum-independent isovector S-wave pion potential but the P-wave component was completely neglected. Motivated by the upcoming data gathering campaign of the SAMURAI TPC collaboration [74], which has among its objectives the experimental measurement of pion emission in heavy-ion collisions of impact energies in the neighborhood of the vacuum threshold for pion production, it is worthwhile to stress once more the importance of including the pion potential with all its components and realistic energy dependence in transport models that attempt to describe such reactions. To that end the impact of the pion potential for two values of the impact energy, $T_{\rm lab} = 250$ MeV/nucleon and $T_{\rm lab} = 400$ MeV/nucleon, in mid-central ^{197}Au $+^{197}$Au collisions is presented in Fig. 16. The strength of the isovector $\Delta(1232)$ potential and the SE stiffness parameter have been set to $V_v = \delta$ and $x = 0$ respectively. For the higher impact energy case, the FOPI-LAND experimental result [22] is also shown for comparison.

Starting with the $T_{\rm lab} = 400$ MeV/nucleon case (right panel of Fig. 16), it is observed that the exclusion of both the S- and P-wave pion potential components leads to significant deviations of the model predictions from the experimental data. This is most evident in the low-p_T region, where the theoretical model overpredicts the experimental data by a factor of four. In the region surrounding the average p_T value the discrepancy becomes an underprediction by a factor of two. Interestingly, the slope of the experimental data is not reproduced by the no-pion-potential version of the model even for the highest accessible p_T values. The situation is considerably improved with the inclusion of the S-wave pion potential, particularly in the large-p_T region where now both the value and the slope of the transverse-momentum-dependent PMR are reasonably close to the experimental data. In the low-p_T region an overestimation of the experimental data by a factor of two persists. This is resolved by the inclusion of the P-wave pion potential (the Batty-1 parametrization in this case), which suggests that the low-energy parts of both the S- and

P-wave potentials are realistic enough. The difference between theoretical and experimental results is however increased in the mid- and high-p_T regions. This result emphasizes once more the importance of the energy-dependent part of the pion potential since for these regions the total pion potential is the result of the subtraction of repulsive *S*-wave and attractive *P*-wave contributions.

These observations are also valid for the case of an impact energy of $T_{\rm lab} = 250$ MeV/nucleon (left panel of Fig. 16) with the important difference that the impact of the pion potential on the PMR increases. In the mid-transverse-momentum region, the inclusion of the *S*-wave potential enhances the PMR by a factor of two; the subsequent addition of the *P*-wave potential leads to a decrease by 20%–30% of this observable. The extraction of a trustworthy narrow constraint for the allowed values for L will thus only be possible with the accurate knowledge and inclusion in the transport model of choice of both components of the pion potential. The smaller differences between these three cases at higher values for p_T is a direct consequence of the cancellation of the strengths of the *S*- and *P*-wave components of the pion potential due to the particular assumed momentum dependence (see Fig. 4).

In contrast to the suggestion put forward or implied by studies of different groups [9,16,17], the results presented above indicate that it may be worthwhile, when attempting to extract the slope parameter L from pion observables, to apply a kinetic energy (or transverse momentum) cut to pion spectra, including only events below a certain maximum value. For the case of kinetic energy spectra a conservative value for this upper limit must not be significantly larger than the kinetic energy of pions in pionic atoms, limiting it to values as low as 20–30 MeV. This ensures that uncertainties in the energy-dependent part of the pion potential are largely removed. Uncertainties in the density dependence above the saturation point of the potential survive and should be removed by means other than kinematical cuts applied on spectra, since it is this density region that provides the interesting physics signal one seeks to isolate. A possible solution to this issue will require identification of heavy-ion observables that present an enhanced sensitivity to the strength of the pion potential and a suppressed one to the quantities of interest. In this context, heavy-ion experimental data for nuclei with small isospin asymmetry may prove valuable.

The present section is concluded with predictions relevant for extracting the density dependence of the SE from forthcoming experimental data of the SAMURAI TPC Collaboration. Measurements of pion production in collisions of various combinations of Sn isotopes for a projectile laboratory impact energy of $T_{\rm lab} = 270$ MeV/nucleon ^{108}Sn + ^{112}Sn have been performed recently [75] and experimental results for the multiplicity and average p_T ratios will presumably become available during the next couple of years. Of these, predictions for those reactions involving nuclei that lead to fireballs with the lowest and highest possible isospin asymmetry, ^{108}Sn + ^{112}Sn and ^{132}Sn + ^{124}Sn (projectile+target), respectively [75], will be presented. The nuclei initialization part of the model has been tuned such as to reproduce, on average, the experimentally measured rms of each of the mentioned isotopes [76] and generate initial density profiles

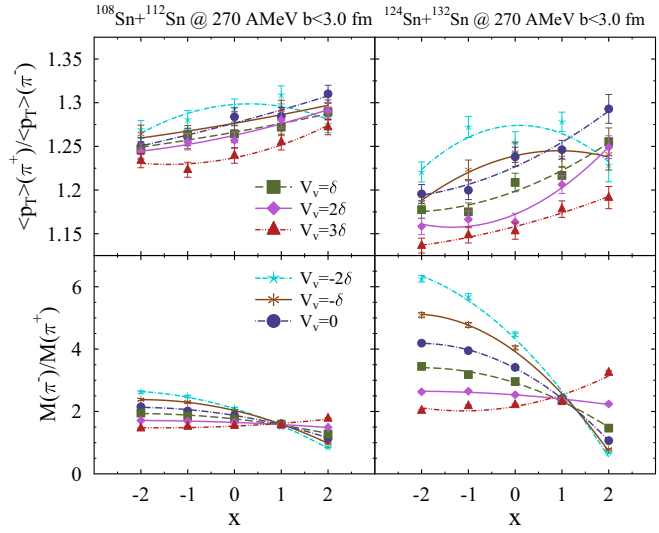

FIG. 17. Theoretical predictions for pion multiplicity (lower panels) and average transverse momentum (upper panels) ratios in ^{108}Sn + ^{112}Sn (left panels) and ^{124}Sn + ^{132}Sn (right panels) central collisions at an impact energy of 270 MeV/nucleon as a function of the stiffness parameter x and for the various choices of the isovector $\Delta(1232)$ isobar discussed in the text. No kinematical cuts have been applied on spectra.

that reproduce a two-parameter Fermi distribution with a diffuseness parameter $a = 0.55$ fm [77].

The predictions for the two mentioned reactions for central collisions ($b < 3.0$ fm) and without any kinematical cuts are presented in Fig. 17. The global energy conservation version of the model, including the effective *S*-wave ChPT inspired and Batty-1 *P*-wave pion potentials, has been employed. The difference in sensitivity to both the isovector nucleon and $\Delta(1232)$ potentials between the low ($\beta = 0.09$) and high ($\beta = 0.22$) isospin asymmetry cases is clearly observed for both the PMR and PAPTR, being significantly more pronounced for the latter isospin asymmetry choice. Compared to ^{197}Au + ^{197}Au collisions at 400 MeV/nucleon impact energy (see Fig. 11) the increase, if any, of the sensitivity of the PMR to the SE stiffness is a function of the strength of the isovector $\Delta(1232)$ potential, being more pronounced for negative values of V_v. For the values of the parameters x and V_v favored by the existing FOPI experimental data the increase of the sensitivity is in the range of 10%–20%. A comparison of PMR with a Δ resonance model predictions that assumes only first chance inelastic collisions [78], $M(\pi^-)/M(\pi^+) = (5N^2 + NZ)/(5Z^2 + NZ) \approx (N/Z)^2$, reveals that these transport model calculations overpredict that result with similar factors for both reactions, similarly to other models [6]. The magnitude of these differences is found to depend on both the SE stiffness and the strength of the isovector $\Delta(1232)$ potential.

V. SUMMARY AND CONCLUSIONS

A QMD-type transport model applicable to heavy-ion collisions with impact energies of a few hundred MeV/nucleon

that allows the conservation of the total energy of the system during such reactions has been further extended by including the effects of the *S*- and *P*-wave components of the pion optical potential. This allows theoretical computations of observables related to the final momenta of the emitted pions. Of these, the final average transverse momenta of charged pions and their ratio (PAPTR) have been studied in detail. The main result of this study is the proof of feasibility of using this observable in conjunction with the charged pion multiplicity ratio (PMR) to extract constraints, from experimental data, for both the stiffness of the symmetry energy and the strength of the isovector component of the $\Delta(1232)$ potential in nuclear matter.

It has been shown that the energy conservation scenarios introduced in a previous study have a significant impact on the ratios of average transverse momenta. Specifically, in the case when the effect of potential energies is not taken into account in the energy conservation constraint appearing in the collision term of the transport equations, the theoretical value of PAPTR is systematically overestimating the experimental one by about 20%. Within the local energy conservation scenario (LEC) the value of PAPTR underestimates the experimental data by a fraction in the range of 5%–10%. Finally, requiring the conservation of the total energy of the system (GEC scenario) leads to an increase of the value of PAPTR such that the experimental data are once again overestimated by an amount in the range of 10%–15%.

The *S*-wave component of the pion potential that has been employed in this study takes into account theoretical results concerning chiral symmetry restoration and pion-nucleon scattering in dense nuclear matter that have been previously validated by the experimental study of properties of pionic atoms. An energy dependence of the potential has been incorporated by using as guidance empirical results about the behavior of the vacuum isoscalar and isovector scattering pion-nucleon amplitudes away from threshold and requiring an agreement with experimental data on pion-nucleus scattering up to pion kinetic energies of 300 MeV.

The *P*-wave pion optical potentials used in this work have their origin in pionic atom studies. Their extrapolation to higher momenta must however be handled with care, given the strong energy dependence of the $\Delta(1232)$ width. To this end the energy dependence of a theoretical model for the optical pion potential derived within the framework of the delta-hole approximation has been mirrored. To be on par with theoretical models describing pionic atom properties, also the density gradient terms of the potential have been implemented in the transport model. They have been shown to have a non-negligible impact on observables in the context of constraining the strength of the isovector $\Delta(1232)$ potential.

The total impact of the *S*- and *P*-wave components of the pion potential on pion multiplicity ratio is found to be moderate. However, by neglecting their contribution, uncertainties that can amount to as much as 50 MeV on the extracted value for the symmetry energy slope at saturation L could be expected, at fixed isovector $\Delta(1232)$ potential strength. The presented model for the pion optical potential leads to a good description of experimental values for the average transverse momenta, at 5% level, in mid-central $^{197}\mathrm{Au}+^{197}\mathrm{Au}$ at an impact energy of 400 MeV/nucleons. The description of the experimental value of the ratio of average transverse momenta of charged pions is of even better quality for certain choices of the *P*-wave optical potential parametrization.

The impact of the strength of the isovector $\Delta(1232)$ potential on the pion multiplicity and average transverse momentum ratios is investigated, confirming the conclusions of a previous study for the PMR and evidencing a similar behavior for the PAPTR. Using available FOPI experimental data for these observables, it is shown that constraints for both the slope L of the symmetry energy at saturation and the strength of the isovector $\Delta(1232)$ potential can be extracted from a two-dimensional χ^2 fit. The inclusion of the *S*- and *P*-wave pion potentials, particularly the former one, is found to be crucial for a simultaneous description of FOPI experimental data for the pion multiplicity and average p_T ratios to be possible for realistic values of the stiffness of the symmetry energy and strength of the isovector $\Delta(1232)$ potential. The obtained values for these parameters are however rather imprecise due to rather large uncertainties that affect the experimental data (multiplicity ratios) and inaccurate knowledge of the pion optical potential for the entire density and energy range probed in heavy-ion collisions.

The presently available experimental data favor a value of the slope parameter L larger than 50 MeV, at 1σ confidence level, implying the claim that the symmetry energy is not soft. The allowed upper limit is however a very stiff one, exceeding the value $L = 150$ MeV for any choice of the *P*-wave pion potential. Additionally, the allowed value for the isovector $\Delta(1232)$ potential strength is, on average, somewhat weaker, by about 25%, than the usual choice employed in transport models. For the favored values for these two parameters, the transport model allows a good description of available FOPI experimental rapidity and transverse momentum multiplicity spectra of charged pions in mid-central $^{197}\mathrm{Au}+^{197}\mathrm{Au}$ collisions at an impact energy of 400 MeV/nucleon.

It has also been shown that by increasing the precision of the experimental measurements the uncertainties of the extracted constraints for the stiffness of the symmetry energy can be significantly reduced. The situation can be further improved by studying experimentally systems with a higher isospin asymmetry at impact energies closer to the vacuum pion production threshold than previously accomplished. For such a program to be successful the knowledge of the pion potential at densities higher than probed in pionic atom experiments and its energy dependence will have to be advanced. This is necessary also because the impact of the pion optical potential increases as the collision energy is decreased. In this context, experimental measurements of reactions involving isospin-symmetric heavy nuclei and restriction of particle spectra to low-kinetic-energy pions may prove helpful.

ACKNOWLEDGMENTS

The research of M.D.C. has been financially supported by the Romanian Ministry of Education and Research through Contract No. PN 16420101/2016. The author would like thank Prof. Dr. W. Reisdorf for providing yet unpublished

FOPI experimental data. The assistance of the DFCTI department of IFIN-HH with the maintenance of the computing cluster on which simulations were performed is gratefully acknowledged.

[1] B.-A. Li, G.-C. Yong, and W. Zuo, Phys. Rev. C **71**, 014608 (2005).
[2] H.-l. Liu, G.-C. Yong, and D.-H. Wen, Phys. Rev. C **91**, 044609 (2015).
[3] B. A. Brown, Phys. Rev. Lett. **111**, 232502 (2013).
[4] Z. Zhang and L.-W. Chen, Phys. Lett. B **726**, 234 (2013).
[5] C. B. Das, S. Das Gupta, C. Gale, and B.-A. Li, Phys. Rev. C **67**, 034611 (2003).
[6] Z. Xiao, B.-A. Li, L.-W. Chen, G.-C. Yong, and M. Zhang, Phys. Rev. Lett. **102**, 062502 (2009).
[7] W.-J. Xie, J. Su, L. Zhu, and F.-S. Zhang, Phys. Lett. B **718**, 1510 (2013).
[8] Z.-Q. Feng and G.-M. Jin, Phys. Lett. B **683**, 140 (2010).
[9] J. Hong and P. Danielewicz, Phys. Rev. C **90**, 024605 (2014).
[10] J. Xu, L.-W. Chen, C. M. Ko, B.-A. Li, and Y.-G. Ma, Phys. Rev. C **87**, 067601 (2013).
[11] B.-A. Li, W.-J. Guo, and Z. Shi, Phys. Rev. C **91**, 044601 (2015).
[12] G.-F. Wei, B.-A. Li, J. Xu, and L.-W. Chen, Phys. Rev. C **90**, 014610 (2014).
[13] G. Ferini, T. Gaitanos, M. Colonna, M. Di Toro, and H. H. Wolter, Phys. Rev. Lett. **97**, 202301 (2006).
[14] T. Song and C. M. Ko, Phys. Rev. C **91**, 014901 (2015).
[15] M. D. Cozma, Phys. Lett. B **753**, 166 (2016).
[16] B.-A. Li, Phys. Rev. C **92**, 034603 (2015).
[17] W.-M. Guo, G.-C. Yong, and W. Zuo, Phys. Rev. C **92**, 054619 (2015).
[18] L. S. Kisslinger, Phys. Rev. **98**, 761 (1955).
[19] M. Ericson and T. E. O. Ericson, Ann. Phys. **36**, 323 (1966).
[20] W. Reisdorf *et al.* (FOPI Collaboration), Nucl. Phys. A **781**, 459 (2007).
[21] W. Reisdorf *et al.* (FOPI Collaboration), Nucl. Phys. A **848**, 366 (2010).
[22] W. Reisdorf (FOPI Collaboration) (private communication).
[23] D. T. Khoa, N. Ohtsuka, M. A. Matin, and R. K. Puri, Nucl. Phys. A **548**, 102 (1992).
[24] V. S. Uma Maheswari, C. Fuchs, A. Faessler, L. Sehn, D. S. Kosov, and Z. Wang, Nucl. Phys. A **628**, 669 (1998).
[25] C. Hartnack, R. K. Puri, J. Aichelin, J. Konopka, S. A. Bass, H. Stoecker, and W. Greiner, Eur. Phys. J. A **1**, 151 (1998).
[26] S. R. de Groot and L. G. Suttorp, *Foundations of Electrodynamics* (North-Holland, Amsterdam, 1972).
[27] C. Xu, B.-A. Li, and L.-W. Chen, Phys. Rev. C **82**, 054607 (2010).
[28] X.-H. Li, W.-J. Guo, B.-A. Li, L.-W. Chen, F. J. Fattoyev, and W. G. Newton, Phys. Lett. B **743**, 408 (2015).
[29] B.-A. Li and X. Han, Phys. Lett. B **727**, 276 (2013).
[30] Z. Zhang and L.-W. Chen, Phys. Rev. C **93**, 034335 (2016).
[31] M. D. Cozma, Y. Leifels, W. Trautmann, Q. Li, and P. Russotto, Phys. Rev. C **88**, 044912 (2013).
[32] P. Russotto, P. Z. Wu, M. Zoric, M. Chartier, Y. Leifels, R. C. Lemmon, Q. Li, J. Łukasik, A. Pagano, P. Pawłowski, and W. Trautmann, Phys. Lett. B **697**, 471 (2011).
[33] K. A. Olive *et al.* (Particle Data Group), Chin. Phys. C **38**, 090001 (2014).
[34] M. Liu, N. Wang, Y. Deng, and X. Wu, Phys. Rev. C **84**, 014333 (2011).
[35] B.-A. Li, Nucl. Phys. A **708**, 365 (2002).
[36] K. Itahashi, K. Oyama, R. S. Hayano, H. Gilg, A. Gillitzer, M. Knülle, M. Münch, W. Schott, P. Kienle, H. Geissel, N. Iwasa, G. Münzenberg, S. Hirenzaki, H. Toki, and T. Yamazaki, Phys. Rev. C **62**, 025202 (2000).
[37] R. Seki and K. Masutani, Phys. Rev. C **27**, 2799 (1983).
[38] C. J. Batty, S. F. Biagi, E. Friedman, S. D. Hoath, J. D. Davies, G. J. Pyle, and G. T. A. Squier, Phys. Rev. Lett. **40**, 931 (1978).
[39] C. J. Batty, E. Friedman, and A. Gal, Nucl. Phys. A **402**, 411 (1983).
[40] J. Konijn, C. T. A. M. de Laat, A. Taal, and J. H. Koch, Nucl. Phys. A **519**, 773 (1990).
[41] N. Kaiser and W. Weise, Phys. Lett. B **512**, 283 (2001).
[42] J. Nieves, E. Oset, and C. Garcia-Recio, Nucl. Phys. A **554**, 509 (1993).
[43] J. Nieves, E. Oset, and C. Garcia-Recio, Nucl. Phys. A **554**, 554 (1993).
[44] M. Doring and E. Oset, Phys. Rev. C **77**, 024602 (2008).
[45] R. Seki, K. Masutani, and K. Yazaki, Phys. Rev. C **27**, 2817 (1983).
[46] K. Masutani and R. Seki, Phys. Lett. B **156**, 11 (1985).
[47] H. Geissel, H. Gilg, A. Gillitzer, R. S. Hayano, S. Hirenzaki, K. Itahashi, M. Iwasaki, P. Kienle, M. Münch, G. Münzenberg, W. Schott, K. Suzuki, D. Tomono, H. Weick, T. Yamazaki, and T. Yoneyama, Phys. Rev. Lett. **88**, 122301 (2002).
[48] K. Suzuki, M. Fujita, H. Geissel, H. Gilg, A. Gillitzer, R. S. Hayano, S. Hirenzaki, K. Itahashi, M. Iwasaki, P. Kienle, M. Matos, G. Münzenberg, T. Ohtsubo, M. Sato, M. Shindo, T. Suzuki, H. Weick, M. Winkler, T. Yamazaki, and T. Yoneyama, Phys. Rev. Lett. **92**, 072302 (2004).
[49] T. Yamazaki, S. Hirenzaki, R. S. Hayano, and H. Toki, Phys. Rep. **514**, 1 (2012).
[50] E. Friedman and A. Gal, Phys. Rep. **452**, 89 (2007).
[51] P. Kienle and T. Yamazaki, Prog. Part. Nucl. Phys. **52**, 85 (2004).
[52] E. E. Kolomeitsev, N. Kaiser, and W. Weise, Phys. Rev. Lett. **90**, 092501 (2003).
[53] C. Garcia-Recio and E. Oset, Phys. Rev. C **40**, 1308 (1989).
[54] C. M. Chen, D. J. Ernst, and M. B. Johnson, Phys. Rev. C **48**, 841 (1993).
[55] C. Garcia-Recio, L. L. Salcedo, and E. Oset, Phys. Rev. C **39**, 595 (1989).
[56] C. Garcia-Recio, E. Oset, L. L. Salcedo, D. Strottman, and M. J. Lopez, Nucl. Phys. A **526**, 685 (1991).
[57] H.-Ch. Schröder, A. Badertscher, P. F. A. Goudsmit, M. Janousch, H. J. Leisi, E. Matsinos, D. Sigg, Z. G. Zhao, D. Chatellard, J.-P. Egger, K. Gabathuler, P. Hauser, L. M. Simons, and A. J. Rusi El Hassani, Eur. Phys. J. C **21**, 473 (2001).
[58] V. Baru, C. Hanhart, M. Hoferichter, B. Kubis, A. Nogga, and D. R. Phillips, Phys. Lett. B **694**, 473 (2011).
[59] V. Baru, C. Hanhart, M. Hoferichter, B. Kubis, A. Nogga, and D. R. Phillips, Nucl. Phys. A **872**, 69 (2011).

[60] C. J. Batty, E. Friedman, and A. Gal, Phys. Rep. **287**, 385 (1997).
[61] M. Krell and T. E. O. Ericson, Nucl. Phys. B **11**, 521 (1969).
[62] S. Weinberg, Phys. Rev. Lett. **17**, 616 (1966).
[63] Y. Tomozawa, Nuovo Cimento A **46**, 707 (1966).
[64] W. Weise, Acta Phys. Polon. B **31**, 2715 (2000).
[65] W. Weise, Nucl. Phys. A **690**, 98 (2001).
[66] E. Friedman, M. Bauer, J. Breitschopf, H. Clement, H. Denz, E. Doroshkevich, A. Erhardt, G. J. Hofman, R. Meier, G. J. Wagner, and G. Yaari, Phys. Rev. Lett. **93**, 122302 (2004).
[67] E. Friedman, M. Bauer, J. Breitschopf, H. Clement, H. Denz, E. Doroshkevich, A. Erhardt, G. J. Hofman, S. Kritchman, R. Meier, G. J. Wagner, and G. Yaari, Phys. Rev. C **72**, 034609 (2005).
[68] E. Friedman and A. Gal, Nucl. Phys. A **928**, 128 (2014).
[69] R. A. Arndt, W. J. Briscoe, I. I. Strakovsky, and R. L. Workman, Phys. Rev. C **74**, 045205 (2006).
[70] O. Buss, L. Alvarez-Ruso, P. Muhlich, and U. Mosel, Eur. Phys. J. A **29**, 189 (2006).
[71] W.-M. Guo, G.-C. Yong, H. Liu, and W. Zuo, Phys. Rev. C **91**, 054616 (2015).
[72] P. Russotto *et al.*, Phys. Rev. C **94**, 034608 (2016).
[73] Y. Wang, C. Guo, Q. Li, H. Zhang, Y. Leifels, and W. Trautmann, Phys. Rev. C **89**, 044603 (2014).
[74] R. Shane *et al.*, Nucl. Instrum. Methods Phys. Res., Sect. A **784**, 513 (2015).
[75] T. Murakami *et al.* (SπRIT Collaboration), Presentation at NuSYM16, Beijing, China, 2016.
[76] I. Angeli and K. Marinova, At. Data Nucl. Data Tables **99**, 69 (2013).
[77] H. De Vries, C. W. De Jager, and C. De Vries, At. Data Nucl. Data Tables **36**, 495 (1987).
[78] R. Stock, Phys. Rep. **135**, 259 (1986).